CoA NOTE AERO. No. 175

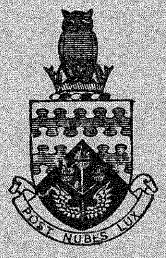

THE COLLEGE OF AERONAUTICS
CRANFIELD

FREQUENCY RESPONSE OF AN AIRCRAFT AS DETERMINED FROM TRANSIENT FLIGHT TESTS USING THE FOURIER TRANSFORMATION METHOD OF ANALYSIS

by

D. W. Laurie-Lean

CoA Note Aero. No. 175

May, 1967

THE COLLEGE OF AERONAUTICS

DEPARTMENT OF FLIGHT

Frequency response of an aircraft as determined from transient flight tests using the Fourier transformation method of analysis

- by -

D.W. Laurie-Lean, A.S.T.C., D.C.Ae., Grad.R.Ae.S.

Ministry of Technology
Contract No. PD/28/028

SUMMARY

The longitudinal dynamic response characteristics of a twin-engined propeller-driven aircraft determined from flight measurements are presented and compared with predictions based on theoretical studies. Transient responses to pilot-applied pulsed motions of the elevator control surfaces were recorded. The transient data was then converted into frequency response form by means of the Fourier transformation and compared with predicted responses calculated from the basic equations of motion of the aircraft.

In particular, detailed experience of the determination of frequency responses with regard to data sampling frequency and control input shape, using the Fourier transformation method, was obtained.

Experimentally-determined transfer functions were used for the evaluation of the stability derivatives that have the greatest effect on the dynamic response of the aircraft.

Some experience was also obtained with automatic data recording and processing equipment using magnetic tape, but no satisfactory frequency responses were obtained using this method. However, with further development and use of this equipment, the analysis of large quantities of flight data would be facilitated.

Contents

List of symbols

a	Lift curve slope of aircraft (rad.$^{-1}$)
$a(\omega)$	Real part of $\frac{\text{output}}{\text{arbitrary input}}$ $(i\omega)$
B	Pitching moment of inertia (slug ft.^{2})
$B = \frac{a}{2} + \nu + \chi,$ $= \frac{a}{2} - \frac{m_q}{i_B} - \frac{m_{\dot{w}}}{i_B}$	Short period damping stability coefficient
$b(\omega)$	Imaginary part of $\frac{\text{output}}{\text{arbitrary unit}}$ $(i\omega)$
$C = \omega + \frac{a}{2}\nu,$ $= -\frac{\mu m_w}{i_B} - \frac{a}{2}\frac{m_q}{i_B}$	Short period stiffness stability coefficient
$C^{\frac{1}{2}} = 2\pi f_o \hat{t},$	Natural undamped short period frequency of the aircraft in aerodynamic time.
$\bar{c}$	Wing mean aerodynamic chord (ft)
$D = d/dt,$	Operator
$F(i\omega)$	Frequency spectrum
f	Frequency (c.p.s.)
g	Acceleration due to gravity (32.17 ft.sec.$^{-2}$)
$h(\omega)$	Real part of $\frac{\text{output}}{\text{step}}$ $(i\omega)$
I	Imaginary part of Fourier transform, $\int_o^T \delta(t) e^{-i\omega t} dt$
I'	Imaginary part of Fourier transform, $\int_o^T \delta'(t) e^{-i\omega t} dt$
$i_B = \left(\frac{k_B}{l_T}\right)^2,$	Coefficient of pitching moment of inertia
k_α	Windvane static position error coefficient
$k_B = \left(\frac{gB}{W}\right)^{\frac{1}{2}}$	Radius of gyration in pitch (ft.)

$k(\omega)$	Imaginary part of $\frac{\text{output}}{\text{step}}$ $(i\omega)$
ℓ_v	Distance of windvane forward of aircraft C.G. (ft.)
ℓ_n	Distance of normal accelerometer forward of aircraft C.G. (ft.)
ℓ_t	Tail arm (ft.)
$\ell(\omega)$	Real part of $\frac{\text{input}}{\text{step}}$ $(i\omega)$
m_w	Pitching moment derivative due to heaving velocity, w.
$m_{\dot{w}}$	Pitching moment derivative to heaving acceleration, $\dot{w}$.
m_q	Pitching moment derivative to rate of pitch, q.
m_η	Pitching moment derivative due to elevator deflection, η.
$m_{\dot{\theta}}$	Complete rotary damping derivative
$m(\omega)$	Imaginary part of $\frac{\text{input}}{\text{step}}$ $(i\omega)$
$n'g'$	Normal acceleration increment above lg.
n_i	Measured normal acceleration
$n_{C.G.}$	Normal acceleration at aircraft C.G.
Δn	Normal acceleration increment
q	Rate of pitch (rad.sec.$^{-1}$)
$\dot{q} = {}^{dq}/_{dt}$	Pitching acceleration (rad.sec.$^{-2}$)
R	Real part of Fourier transform, $\int_o^T \delta(t)e^{-i\omega t}dt$
R'	Real part of Fourier transform, $\int_o^T \delta'(t)e^{-i\omega t}dt$
$R(\omega)$	Amplitude ratio of output to input
S	Wing area (ft.^{2})
$t = \hat{t}\tau$	Time (secs.)
$\hat{t} = \frac{W}{g\rho SV}$	Unit of aerodynamic time
T	Time (Secs.) as a limit of integration.

V	Forward velocity of aircraft in undisturbed flight (ft.sec.$^{-1}$).
W	Weight of aircraft (lbs.)
w	Increment of velocity along Z axis in disturbed flight (ft.sec.$^{-1}$)
$x = \frac{2\pi f t}{C_{\frac{1}{2}}}$	Non-dimensional frequency of short period oscillation.
$x(t)$	Input transient
$x'(t)$	Derivative of input transient
$y(t)$	Output transient
$y'(t)$	Derivative of output transient
Z_n	Distance of normal accelerometer above aircraft C.G. (ft.)
Z_w	Normal force derivative due to heaving velocity, w.
α	Aircraft incidence (rad.)
$\alpha(\omega)$	Phase difference between output and input
$\Delta\alpha = (\frac{w}{V})$	Incremental aircraft incidence (rad.)
$\alpha_{C.G.}$	Aircraft incidence at the C.G. (rad.)
α_v	Windvane incidence (rad.)
δ	Elevator moment coefficient
$\delta(i\omega)$	Frequency response function
$\delta(t)$	Transient
$\delta'(t)$	Derivative of transient
$\lvert\delta\rvert$	Magnitude of Fourier transform $\int_o^T \delta(t)e^{-i\omega t}dt$
$\lvert\delta'\rvert$	Magnitude of Fourier transform $\int_o^T \delta'(t)e^{-i\omega t}dt$
$\zeta = \frac{B}{2C_{\frac{1}{2}}}$	Short period damping ratio (ratio of actual to critical damping).
$= \zeta_a + \zeta_v + \zeta_\chi$	

$\zeta_a = \frac{a/2}{2C_{\frac{1}{2}}}$ Lift contribution to damping ratio

$\zeta_\nu = \frac{\nu}{2C_{\frac{1}{2}}}$ Rate of pitch contribution to damping ratio

$\zeta_\chi = \frac{\chi}{2C_{\frac{1}{2}}}$ Rate of change of incidence contribution to damping ratio

η Elevator deflection (rad.)

θ Angular displacement in pitch from equilibrium position (rad.)

$\theta_i(t)$ Arbitrary input

$\mu = \frac{W}{g\rho S l_T}$ Aircraft density parameter

ν Rotary damping coefficient

ρ Air density (slugs.ft.$^{-3}$)

ϕ Phase angle (deg.)

χ Rate of change of incidence damping coefficient

ω Angular frequency (rad.sec.$^{-1}$)

ω_ν Method function frequency (rad.sec.$^{-1}$)

1. Introduction

Measurements of aircraft frequency response from flight data is becoming an increasingly important method of obtaining a complete dynamic description of the aircraft. Conventional techniques for obtaining stability derivatives, such as free oscillation, time vector diagrams, matching, and equations of motion methods, are inadequate, because they either yield insufficient information or because they have other limitations on their use.

The direct method of obtaining frequency-response data by sinusoidal oscillation of the control surface at varying frequencies is impractical from the points of view of time and expense. Not only is this method expensive in terms of flight time, but it requires the complexity of an autopilot input together with a sinusoidal function generator.

An alternative method for determining the frequency response is the transient response method, which entails measuring the aircraft transient responses to pilot-applied inputs. The aircraft frequency response can be obtained from the transient response by a number of methods, the relative merits of which are discussed in the next section. The prime purpose of these tests, however, was to study the Fourier transformation method and its limitations in obtaining the frequency response from the transient response.

2. Review of methods

2.1 Sinusoidal response method.

2.2 'Curve-fitting' methods.

2.3 Fourier methods.

2.4 Shinbrot's method.

2.5 Cross spectral analysis.

2.1 Sinusoidal response method

The most direct method of obtaining the aircraft frequency response is to oscillate the control surface sinusoidally at a constant amplitude and frequency until a steady-state response of the aircraft has been obtained, and then to measure the amplitude and phase relationship between input and output sine waves. This process is repeated at different frequencies throughout the frequency range of interest as described in references 1 and 2.

Although the sinusoidal response method requires the least amount of computation time, it is the most extravagant in terms of the flight time involved. An attempt to reduce the flight time involved by the use of a manual frequency sweep technique, as described in reference 3, has met with a moderate amount of success.

2.2 'Curve-fitting' methods

In the so-called 'curve-fitting' methods the form of the transfer function is assumed, either directly or indirectly, and the coefficients of the transfer function are then determined either by direct computation or by least-squares methods, the transfer function often being obtained without first obtaining the frequency response function. The two main 'curve-fitting' methods are the exponential-approximation method and the Donegan-Pearson method.

The exponential-approximation method, described in references 1, 2 and 4, solves for the coefficients of analytical expressions which approximate the time histories of the input and output functions. Since the response of a linear system to a step or impulse is a sum of exponentials, then the choice of exponential terms for fitting aircraft time response is an obvious one. The number of exponentials is selected so that the Laplace transformation will give the same polynomial expressions as obtained from stability theory. The transfer function is then established by taking the Laplace transform of these analytical functions. This method can only be applied for inputs which have a Laplace transform. In the case of lightly damped systems, the damping and stiffness coefficients in the transfer function can be obtained directly from consideration of the period of the oscillation of the transient response and the time for it to damp to half amplitude. For highly damped systems, a least squares method for obtaining the period, damping and other coefficients of the response is necessary.

The Donegan-Pearson method, described in references 2 and 5 requires a direct assumption as to the form of the transfer function and it solves for the coefficients by substituting the input and the output time functions and their integrals into the transfer function. This method is appropriate for obtaining the transfer function from transient response to an arbitrary input. The expression of the transfer function in integral form is an important point with regard to the application of this technique as the integration processes are inherently more accurate than the differentiation process indicated in the normal form of the transfer functions. The integrals and the coefficients may then be obtained by matrix methods.

In both these 'curve-fitting' methods, the order of the expressions used to approximate either the transfer function or the transient responses is unlimited. The assumption of the form of the transfer function therefore does not appear to be particularly restrictive providing that the system is linear. The least-squares computation does, however, increase rapidly with increase in the order of the equations and also the equations themselves tend to become progressively more ill-conditioned. In general, it is necessary, therefore, to neglect low-frequency (phugoid) modes and high-frequency (structural) modes in order to hold the order of the equations at a reasonable level.

2.3 Fourier transform method

The frequency response of a system may be obtained from the ratio of

the Fourier transform of the output transient to the Fourier transform of the input transient as follows:

$$F(i\omega) = \frac{\int_o^\infty ye^{-i\omega t}dt}{\int_o^\infty xe^{-i\omega t}dt}$$

Integration of the Fourier integral offers a choice of methods which may be divided into two general categories.

The first, described in reference 7, is one in which the transient is divided into finite intervals and approximated within each interval by an analytical expression. The integration process may then be performed analytically. A choice of the form of the analytical representation must be made, the accuracy of the determination of the frequency response increasing as the chosen representation becomes more complex. However, as the analytical representation increases in complexity, the computational time also increases at a rapid rate. A compromise is therefore necessary and the simplest expression usually chosen is a cubic, as it is the lowest order polynomial that contains a point of inflexion.

The second category of methods are those in which $e^{-i\omega t}$ is expressed in trigonometric form as shown in references 2 and 7. The resulting sine and cosine functions are multiplied by the values of the transient at corresponding times, and the product curves integrated to determine the real and imaginary parts of the Fourier integral. A modification of the frequency response function uses the time derivatives of the input and output functions instead of the functions themselves, e.g.

$$F(i\omega) = \frac{\int_o^\infty y'e^{-i\omega t}dt}{\int_o^\infty x'e^{-i\ t}dt}$$

The advantage of expressing the frequency response function in this form is the removal of the 'd.c. error' in cases where the trim conditions at the beginning and end of a 'run' are not the same. This form of the frequency response function can be used with any data for which the input and the output begin and end in a steady state. The disadvantage of this form, however, is associated with attendant inaccuracies of the inherently 'noisy' differentiating processes. Potentially, at least, Fourier analysis will detect all details of the frequency response, such as phugoid and structural modes, which are within the accuracy of the measurements and the calculation procedure.

It is this latter form of Fourier analysis that is the basis of the work in this report. Some experimental results obtained using the Fourier method of analysis are contained in references 6 and 8.

2.4 Shinbrot's method

The shinbrot method of reference 9 is basically an equations-of-motion method in which the aircraft stability derivatives, or groups of derivatives, are obtained directly without reference to the frequency response function. Because it is used to analyse forced responses Shinbrot's method enables a larger number of derivatives, including control derivatives to be obtained. An assumption is required as to the form of the equations of motion to be used and the method can be applied to linear or non-linear equations. In the latter case the non-linear terms are usually represented by third order polynomials.

Shinbrot's method is a logical development of the Fourier transform method and is intended to remove some of the limitations of that method. Each equation of motion is treated separately and is multiplied by a number of 'smooth' functions of time, known as 'method functions'. These method functions are usually of the form $\sin^n \omega_v t$ and replace the sin ωt functions of the Fourier transform method. This form of the method function eliminates the dependence on initial and final conditions, the dependence on initial conditions being removed by elimination of the cosine functions. Dependence of the equations on time derivatives of the recorded data is eliminated by the successive integration by parts, the power 'n' in the method function being chosen to be the same as the highest order derivative occurring in the equation of motion. In this way each term is now the product of two independent functions of time, the part containing the recorded data being integrated, and only the part consisting of the method function itself being differentiated. The elimination of dependence on initial conditions in this way results in a heavy dependence on final conditions. However, a careful choice of frequencies eliminates this dependence on final conditions.

The process produces a redundant number of linear simultaneous equations. The coefficients of these equations are integrals of the recorded data, and after these integrals have been evaluated, the equations are solved by least squares to obtain the unknowns.

2.5 Cross Spectral Analysis

Analysis by the cross spectral density technique as described in references 10 and 11 is a means of directly obtaining the frequency response from transient data. This method has the advantage that it tends to reject any part of the output transient which has not been caused directly by, and is therefore statistically independent of, the deliberate input transient. The spurious effects of noise or turbulence are therefore suppressed.

The powerful methods of power spectral analysis require an input which has a high harmonic content at all frequencies over the range of interest. The alternatives for providing such an input are the complexity and expense of an airborne function generator with the characteristics of an autopilot, or a pilot-applied random-appearing input with all its power concentrated in, but spread evenly over, the frequency range of interest.

It is possible to check the dependency of the output transient on the input by means of the coherency function. If the output transient is derived completely from the input transient through a linear transfer function, then the coherency function will be unity. For completely independent input and output transients, the coherency will be zero. Therefore, when the spectra and hence the aircraft response is computed, a check should be made to ensure that the coherency is nearly unity.

3. Test method and equipment

3.1 The aircraft was a twin-engined Hawker Siddeley 'Dove' Mk. 5 aircraft, powered by two Gipsy Queen 70 Mk. 2 piston-engines (Figures 1 and 2). The physical characteristics of the aircraft are listed in Appendix I.

The test method was as follows: The test aircraft was flown at an altitude of 7,000 feet and trimmed at an indicated airspeed of 150 knots in smooth conditions. The galvanometer trace recorder was switched on at the beginning of each run and switched off at the end of each run, whereas the magnetic tape recorder ran continuously. The beginning and end of each run was marked on the magnetic tape by the pilot's commentary. During each test run the elevator was deflected and then returned to the trim position until the oscillatory motion of the aircraft had subsided. In some early development flights, however, the pilot had experienced some difficulty in returning the aircraft to the trimmed condition at the end of each manoeuvre, and so a simple gunsight with collimating lens to avoid parallax effects was mounted above the instrument panel. This provided the pilot with an attitude reference with respect to the horizon and also enabled him to make a crude assessment of the amplitudes of the aircraft responses. Various types of pilot-applied inputs were tried, including pulses, triangular inputs, doublet inputs and frequency sweeps. Examples of these inputs may be seen in figures 15 to 18 inclusive.

3.2 Aircraft instrumentation

The aircraft was fitted with a nose boom on which were mounted windvanes for sensing sideslip and angle-of-attack, as shown in Figure 3. These vanes were fitted with Penny and Giles inductive pick-offs. Pitch rate was sensed by a Smiths RGS/1 rate gyroscope of ± 20 deg.sec.$^{-1}$ range, which had temperature-compensated fluid damping. Normal acceleration was sensed by an R.A.E. type accelerometer with an inductive pick-off and eddy current damping. The normal accelerometer range was 0 to 2g. The elevator deflection was sensed by a Penny and Giles rectilinear potentiometer.

The pitch rate gyroscope and normal accelerometer were mounted on a machined plate (Figure 4) which was situated on the axis of symmetry of the aircraft at a chordwise position of 0.33 $\bar{c}$. All sensors were aligned to within 0.10 degrees with respect to aircraft axes. This was done by using a precision spirit level on the datum points of the wing main-spar in the fuselage, ensuring by the aid of a theodolite that these datum points were on a level parallel to the wing tips. The machined mounting plate for the

transducer package was then aligned to the main-spar datums. The same process was employed in the longitudinal sense using the datum pegs on the fuselage side.

3.3 Instrumentation calibration

All sensing instruments were statically and dynamically calibrated. The static calibrations of the pitch rate gyroscope and the normal accelerometer were carried out on a rate table and whirling arm respectively. The wind vane and the elevator control surface potentiometer were statically calibrated in situ on the aircraft using protractor-type jigs. In the case of the wind vane, the zero position with respect to aircraft axes was determined with the aid of a theodolite.

The dynamic phase angle response of each sensor and its associated electronics was measured on a compound pendulum with displacement and velocity pick-offs as described in reference 12. The galvanometer trace recorder, used for recording the flight data, was also used to record the instrumentation calibration data. In this way the complete instrumentation system used for the calibrations was exactly the same as that used for data acquisition. The resulting phase angle responses are shown in Figures 5 and 6.

In addition, the aerodynamic response of the wind vane to a step input was measured in flight. The aircraft was trimmed in smooth air at the test height and airspeed and the incidence vane was deflected from its equilibrium position and released. The resulting damped oscillation of the vane was recorded on the galvanometer trace recorder and is shown in Figure 7. The resulting aerodynamic properties of the vane are given in Appendix 2.

The aerodynamic static position error (figure 8) resulting from the distortion of the airflow direction by the aircraft at the vane position, was determined from partial glide tests as shown in Appendix 2.

A complete summary of the errors and corrections involved in the determination of the aircraft frequency response is found in Appendix 2.

3.4 Data recording

The aircraft transient responses in incidence, pitch rate, and normal acceleration, as well as the pilot-applied elevator input, were recorded on a Technical and Research Processes Ltd. Type 8-2 12-inch continuous galvanometer trace recorder (figure 9). The signals from the transducers were conditioned by active filters having a cutoff at 15 c.p.s. and were recorded both before and after filtering. This made it possible to see the amount of 'noise' present in the system. A paper trace speed of 6 inches per second was used for recording and a time marker was applied to the trace every one-tenth of a second.

A magnetic-tape data-recording system (figure 9) was operated in parallel with the continuous trace recorder. This system was developed at The College

of Aeronautics and is known as the Cranfield Airborne Digital Data Instrumentation System (CADDIS). Digital recording in flight preserves the accuracy and integrity of the recording in any subsequent handling which may take place in the ground replay equipment, and it also enables the use of a tape transport mechanism in the aircraft which is less liable to introduce errors in the recording process than comparable analogue systems (reference 14). The digital machine, being simpler, is more able to withstand the aircraft environment than the conventional precision tape transports which are required for analogue recording. However, the advantages of analogue recording and display are maintained by CADDIS in the form of a 'quick look' facility.

The signals from the transducers were converted from analogue to digital form (pulse code modulation) and recorded on a time-sharing basis on the channels of a magnetic tape recorder. For ease of handling, the high-level signals from the transducers were scaled to between 0 and 1 volt by means of simple attenuators. Also, because the transducers had inductive pick-offs, demodulators were interposed between the pick-offs and a multiplex unit which was responsible for sequencing the time-sharing channels and for the frequency of data sampling. The signals then passed through an analogue-digital converter before being stored in digital form on the airborne tape recorder. The master time reference for the sequential pulse generators was provided by a 120 kc/s crystal clock. The magnetic tape had sixteen channels of which five were available for direct frequency modulation analogue recording and one for speech commentaries. Of the primary channels, one was for the parity signal, one for synchronisation, and the remaining eight were used for the digital data output. The frames of ten channels were recorded sequentially in 1/150 seconds. For the work in this report only four of these channels were used and the time delay between channels one and four was 1/500 second.

3.5 Data Processing

The galvanometer trace records of elevator input and aircraft transient responses were converted from analogue to digital form using a Benson-Lehner 'Oscar' trace reader as shown in Figure 10. The traces were sampled at time intervals of one-fiftieth of a second and scaled according to the instrumentation static calibrations. The data was produced on punched paper tape together with a printout for checking and editing purposes. The best indication of where to end the run was when both zero pitch rate and unit normal acceleration had been reached.

In the case of the magnetic tape data, the tape from the airborne recorder was replayed on the ground installation, shown in Figure 11, in 'real-time' ($7\frac{1}{2}$ ins./sec.) to ascertain the start and end of each run using the pilot's commentary as a guide. From this 'real-time' replay, a 'quick-look' record was produced by passing the data through a digital-analogue converter synchronised with the channel selector and feeding a ten-channel sample-and-hold circuit, the outputs of which were fed to a ten-channel galvanometer trace recorder. This trace record was then used to determine the exact beginning and end

positions of each run to be analysed.

Using these beginning and end positions, the magnetic tape was again replayed at a speed reduced by a factor of 32 (i.e. 15/64 ins./sec.) so as to permit asynchronous operation with the high speed paper tape punch. The need to reduce the magnetic tape speed made it desirable to use the most efficient paper tape format possible, and so the standard binary-coded decimal tape form was abandoned in favour of retaining the data as an 8-bit binary number. The 'raw' data was thus obtained on punched paper tape at a sampling rate of 150 times per second. The instrumentation calibrations, represented by a seventh order polynomial equation were then incorporated using a calibration sub-routine programme on the 'Pegasus' computer. A simple translation programme was used to convert the data from the binary form to decimal form, ready for analysis.

Simple programmes were also used in some cases, as explained in sections 5 and 6, to apply instrumentation dynamic calibrations and position error corrections to the data before analysis.

4. Method of Analysis

The Fourier method of analysis (Reference 15) was used to write a machine code programme for use on the 'Pegasus' computer (Figure 12). The basic principle of the method depends on the fact that a step function may be approximated by a Fourier series; by superposition, the transient responses may therefore be approximated by a series of step functions (Figure 13). The arbitrary control surface input, and each resultant transient responses, were thus expressed as a series of step functions in the form of trigonometric series. Use was then made of the fact that the frequency-response function is equal to the ratio of the Fourier transform of the output transient to the Fourier transform of the control surface input, as follows:-

$$F(i\omega) = \frac{\int_o^\infty y e^{-i\omega t} dt}{\int_o^\infty x e^{-i\omega t} dt}$$

This form of the frequency-response function is restricted in the cases of finite records, as mentioned in Section 2.3, in which the trim conditions at the beginning and end of the 'run' are not the same. This problem was overcome by using the derivatives of the input and output functions in the Fourier transform as follows:-

$$F(i\omega) = \frac{\int_o^\infty y' e^{-i\omega t} dt}{\int_o^\infty x' e^{-i\omega t} dt}$$

In this case it was only necessary for the runs to begin and end in a steady state (i.e. $x' = 0$ and $y' = 0$). An outline of the method is given in Appendix 3.

5. Results and Discussion

5.1 Trace records

A typical galvanometer trace record, taken on the 5th run of flight 7, is shown in figure 14. The lack of 'noise' in the system is readily seen from a comparison of the filtered and unfiltered signals. It was considered justifiable, therefore, to analyse the unfiltered data.

On some early development flights, however, some noise was encountered due to the aircraft engine vibration affecting the galvanometer trace recorder. This effect was eliminated in subsequent flights after a modification to the trace recorder mounting.

5.2 Inputs and harmonic content

Examples of some of the elevator control surface inputs used are shown in figures 15 to 18 inclusive, and the harmonic content of these inputs over the frequency range 0.5 to 15.0 rads/sec. is shown in figures 19 to 22 inclusive. It can be seen in figure 19 that the long-duration 'doublet' type inputs of figure 15 consistently have a high harmonic content at frequencies centred around 5 and 11 rads/sec., and low harmonic content in the region centred around a frequency of 8 rads/sec. The short duration pulses of figure 16 have a harmonic content (figure 20) which increases almost linearly with frequency over the range under consideration.

Figure 17 shows inputs that were intended to provide a reasonably constant harmonic content over the frequency range of interest. These 'frequency-sweep' inputs did in fact have a high harmonic content over most of the frequency range (figure 21), but the content was low around the aircraft short period frequency of approximately 3 rads/sec. and was not a 'smooth' function of frequency. Figure 18 shows 'doublet' inputs of short duration, most of which have a high harmonic content over the frequency range (figure 22), although these are not always smooth functions of frequency.

In general, simple short-duration pulse type inputs yield harmonic contents which increase steadily with frequency. The larger input amplitudes usually give higher harmonic content at a given frequency due to the greater energy input into the system. The simpler the type of input shape (e.g. short duration pulse input), the smoother is the harmonic content relationship as a function of frequency.

5.3 Frequency responses

The frequency-response functions resulting from the inputs of Figures 15 to 19 are shown in Figures 23 to 34 inclusive. Some of these responses display peaks in the curves at certain frequencies (as for example in Figures 23 to 25 inclusive, flight 21, run 8, at a frequency of 14 rads/sec.) where the harmonic content of the input is low. This shortcoming in the

method can be overcome by applying various types of inputs to the aircraft, or inputs of various duration, in order to cover any regions of uncertainty thus ensuring that no legitimate secondary peak or other significant characteristic exists in the region of that particular frequency. Halving the duration of a pulse input, for example, has the effect of doubling the spacing between frequencies of low or zero harmonic content.

An ideal impulse-type input would, of course, have equal harmonic content at all frequencies, but in practice the duration of the input must be sufficient to ensure accurate measurement of the response. Hence any practical input will have low harmonic content at some recurring multiples of frequency. From a survey of the results obtained it is not possible to determine a unique level of harmonic content below which unreliable frequency response results are obtained. However, an approximate indication of the minimum level of harmonic content required for reliable results is shown in figures 19 to 22.

A comparison is given in Appendix 4 of the harmonic content distribution with frequency for typical triangular inputs between the case in which the Fourier transform is expressed in terms of the input transient itself and the case in which it is expressed in terms of the derivative of the transient. It may be seen from this comparison that the requirements of an input, in terms of harmonic content, for both forms of the Fourier transform are different at the low frequency end. A shorter duration pulse is required, when the derivative form of the input transient is used, in order to establish sufficient harmonic content in the region of the short period mode natural frequency.

5.4 Repeatability

Figures 23 to 34 show that, for similar inputs at least, reasonable repeatability of the frequency response function was achieved. In fact, in the regions where the frequency response function results were reliable, there was still reasonable repeatability even when the results from dissimilar inputs were compared.

5.5 Sampling frequency

Figure 35 shows the effect of the sampling frequency of the data on the frequency response function. This figure shows the frequency response function for sampling time intervals of 0.02 and 0.10 seconds. It can be seen that up to a sampling time interval of 0.10 seconds that a degree of consistency in the results was maintained. The phase angle responses are little affected by the increase in sampling time interval whereas the amplitude ratio responses are mainly affected at frequencies below the short period natural frequency. For the input (Flight 7, run 5) corresponding to the frequency response of figure 35, the sampling time interval would have to be increased still further before any gross inaccuracies occurred due to aliasing. For pulse inputs of longer duration the sampling time interval could be increased even further before degradation of the results occured due to aliasing.

5.6 Dynamic and position errors

Figure 23 to 34 show frequency responses as determined from 'raw' data. Figure 36 shows the effect of inclusion of instrumentation dynamic and position error corrections. As described in detail in Appendix 2, the dynamic error corrections due to phase lags in the instrumentation system were incorporated by shifting the data time scale. It can be seen from figure 36 that these dynamic error corrections, as might be expected, have little effect on the amplitude ratio responses and only serve to reduce the phase lag responses linearly with frequency when compared with the 'raw-data' responses.

The position error corrections only affect the incidence and normal acceleration responses, and their sources are explained in Appendix 2. The corrections to the normal acceleration data make only a few degrees difference to the phase angle response and negligible difference to the amplitude ratio response. In the case of the incidence, however, the amplitude ratio response is only affected at frequencies less than the short period, whereas the phase lag is increased throughout the frequency range by approximately 15 degrees from the short period frequency onwards and tapers off to zero at the low frequency end.

5.7 Theoretical frequency response

Figure 37 shows a comparison of the measured frequency response (flight 7, run 5) and the calculated frequency response corresponding to equations 2 and 3 of Appendix V. The calculated frequency response was matched to the measured response by making use of the fact that the phase lag is always 90 degrees at the damped natural frequency and that the corresponding amplitude ratio is equal to $(\frac{1}{2\zeta})$. Hence the damping was calculated and the value of C was then estimated from the measured response. The value of B was determined from the damping ratio, ζ, and with B and C known the elevator moment coefficient, δ, was then evaluated.

As would be expected with matched curves the area of close agreement centres mainly around the matched point, in this case being at the damped natural frequency. Elsewhere there is some deviation which is not entirely outside the experimental accuracy. Possibly a better matching technique would be a least-squares fit to the theoretical curve.

The following results include the main short period coefficients and derivatives corresponding to the matched theoretical frequency response curves of figure 37.

Aerodynamic time, $\hat{t}$	1.44 secs.
Damped natural frequency, $f_{(\varphi = -90°)}$	2.90 rad. sec^{-1}
Short period stiffness stability coefficient, C	18.15
Aircraft density parameter, μ	17.70
Short period damping stability coefficient, B	5.32
Short period damping ratio, ζ	0.62
Rotary damping derivative, $m_{\dot{\theta}} = (m_q + m_{\dot{w}})$	-0.276
Elevator moment coefficient, δ	28.30
Pitching moment derivative due to elevator, m_η	-0.15

$$m_w + (0.136)m_q = 0.1$$

5.8 Test function

The transient response of a second-order system to a step input was used as a test function in order to check the Fourier transformation computer programme, and also to study the effect of reading errors due to the human operator using the Benson-Lehner trace reader. The step input and theoretical transient responses for damping ratios of 0.1, 0.2 and 0.5 were read on the Benson-Lehner trace reader in a similar manner to the aircraft responses. The resulting data tape was then analysed, using the Fourier transformation programme, in order to obtain the second-order system frequency responses. These frequency responses are shown in figures 38 and 39 together with the theoretical second-order system frequency responses. Figure 40 shows the measured frequency responses for a damping ratio of 0.10 for various truncated transient response record lengths. It is seen that the measured responses have a 'waviness', the amplitude of which increases with frequency and with the amount of truncation of the record length. Figure 41 shows the Fourier transform of the trace-read step input compared with the theoretical input transform. The 'waviness' of the trace-read input transform is due to the Benson-Lehner reading errors (which are usually less than 5 parts in 1,000). The 'waviness' is seen to increase with frequency.

5.9 Experience with a digital recording system

Development problems with the CADDIS digital system precluded the obtaining of any reliable frequency response results from this equipment. However, as a result of the limited experience with CADDIS, some ideas on the characteristics required of a digital recording system were obtained.

The dynamic range of the signal which is to be recorded by the system is usually difficult to specify in practice. Estimates of maximum values to be measured usually increase and, in addition to this, allowance must be made for the poor saturation characteristics of flight test recording systems. That is, a very small part of the linear recording range is sacrificed so that the dynamic range which is measured as the ratio of the full scale signal to the threshold noise level can be improved.

The resolution of the measuring system is important, and unfortunately precise statements cannot be made about the resolution required since essentially a signal is being recovered from a combined noise plus signal where the noise may be from both correlated and uncorrelated sources. The ability to recover the signal relies therefore on the noise itself and on the analysis technique employed in the data reduction. Also, if averaging a correlation between two signals takes place in the analysis process, as is the case in frequency response testing, then the effect of the noise is less important than in the case where discrete measurements are made.

The CADDIS digital system using 8 bits actually has a resolution which is less than that of the analogue system using the Benson-Lehner 'Oscar' trace reader. The analogue system therefore has smaller quantisation noise but has an additional source of noise, namely, that due to the human operator in the reading process. Thus although the resolution can theoretically be up to eight times greater using the semi-automatic trace reader, this is never realised in practice. However, the ability to adjust the dynamic range after recording with the analogue system, is of great value.

Although in some types of encoder the resolution equals the accuracy, this is not always the case and therefore should not be the over-riding factor which dictates the choice of a particular system. In many cases the whole system may be self-calibrating due to the time multiplexing which is used and therefore long-term accuracy or stability may be relatively unimportant. In flight testing, the resolution of the recording system is often the dominant factor in assessing the system suitability for a particular test and this is especially true in the measurement of stability and handling characteristics of the aircraft over a wide range of flight conditions. The accuracy can be no better than the resolution and the dynamic range of the signal will determine the smallest digital value which can be assigned to it.

In normal use, the tolerance on the full-scale value set by the flight test requirement plus the additional margin of error and/or tolerance in setting up the system by the instrumentation engineer means that it is unlikely in practice that more than about seventy percent of the available recording range will be used. This figure also takes into account the fact that in many tests, the mean value of the signal may change considerably with different flight conditions.

If the desired minimum value is related to the usable full-scale value then the relationship between resolution and full-scale value can be seen in the following table for three different encoders

No. Bits	Full Scale Digital Capacity	Usable Range 70%	Desirable Min. Value (1/20 max)	Resolution at this Value (%)
8	256	180	9	10
9	512	360	18	5
10	1024	720	36	3

It is evident from this somewhat simplified analysis that the figure of 8 bits may be insufficient for many flight test purposes. In particular in the work of this report the effect is to raise the requirements on the minimum power content at a particular frequency for confident prediction of a point on the system frequency response.

6. Future work

Future research into the determination of the frequency response function from transient tests should involve a more mathematical study of the Fourier transformation process itself. This would include a study of the effect of 'noise' on the transformation process in order to establish some minimum criteria with regard to signal to noise ratio.

A comparative study of the results using the Fourier transformation process based on the transients themselves and on the derivatives of the transients using the same flight test records would also be of great value.

Development of the cross spectral methods of obtaining frequency response is important as with this method the detection of unreliable or spurious results by means of the 'coherency' function is possible. The spectral techniques require the use of a random input and this would suggest a method whereby a 'white' noise input (the statistical properties of which are known) is applied to the aircraft by means of the autopilot. This would enable the aircraft system to be analysed whilst apparently flying on a straight and level course.

Improvements in data recording and processing would seem to lie in the development of an adaptive 'floating point' digital data recording system which would enable the dynamic range to be adjusted to the maximum so as to reduce the effect of noise due to quantisation. It would also seem apparent that in order for such automatic data recording systems to compete with semi-automatic equipment in terms of accuracy, the full scale digital capacity would have to be increased to something like 10 bits.

7. Conclusions

1. The longitudinal dynamic response characteristics of the Hawker Siddeley 'DOVE' Series 5 test aircraft were determined from transient flight tests using the derivative form of the Fourier transformation method of analysis.

2. It was found that simple short-duration pulse-type inputs, having harmonic contents which increase steadily with frequency, yield reliable frequency response functions in the region of the short period natural frequency.

3. It was found from experience of the derivative form of the Fourier process that the minimum value of harmonic content of inputs required to yield reliable frequency response functions is given by the relationship: $|\delta'| = 0.02 + 0.083f$ (where f is expressed in radians per second). Also the harmonic content of the input must be a smooth function of frequency.

4. The longitudinal responses for the test aircraft were matched by simple second-order system transfer functions determined from the linear equations of motion.

5. The sampling time interval must be sufficiently small (a) to avoid aliasing effects, and (b) to ensure that a sufficiently accurate representation of the transients is used in the numerical integration process.

For the short-duration pulse inputs used in this report a sampling time interval of 0.05 seconds fulfilled these requirements.

Appendix I

Physical characteristics of test aircraft

Test aircraft — Hawker Siddeley 'Dove' Series 5.

Power plant — Two Gipsy Queen 70 Mk.2 six-cylinder in-line inverted aircooled piston engines rated at 355 b.h.p. at 4,250 feet.

Wing

Total area	335 ft^2
Span	57 ft.
Aspect ratio	9.7
Taper ratio	0.288
Mean aerodynamic chord	5.88 ft.
Dihedral	4 deg.
Aerofoil section	Piercy
Total aileron area	10.9 ft^2

Horizontal tail

Total area	35.46 ft^2
Elevator area	24.50 ft^2

Vertical tail

Total area	20.40 ft^2
Rudder area	13.75 ft^2

Weights

Flights 7 and 8	8532 lbs.
Flights 9 and 10	8422 lbs.

Centre of gravity

Flights 7 and 8	0.322 $\bar{c}$
Flights 9 and 10	0.179 $\bar{c}$

Coefficient of pitching moment of inertia, $i_B = 0.095$

Appendix II

Errors and corrections involved in the determination of aircraft frequency response from transient flight tests

There are four sources of error in the measurements which might be significant over the range of frequencies considered. These are errors due to the static calibrations of the transducers, errors due to the dynamics of the instrumentation, the unsteady aerodynamic position error of the incidence vane, and kinematic errors due to the geometrical positions of the transducers away from the aircraft centre of gravity.

Errors due to instrumentation static calibrations

In the case of the galvanometer trace-recorded data, the static calibrations are incorporated inherently in the setting up of the Benson-Lehner 'Oscar' trace reader. Thus the data tape outputs of the trace reader automatically incorporate the static calibrations.

In the case of the magnetic tape data, which is converted in the 'raw' data form to punched paper tape from via CADDIS, the instrumentation static calibrations are expressed in the form of a seventh order polynomial and incorporated by means of a computer programme using the Ferranti 'Pegasus' computer.

Errors due to instrument dynamics

The dynamics of the windvane, pitch rate gyroscope and normal accelerometer, each with their associated intermediate circuits, was determined using a compound pendulum with displacement and velocity pickoffs, as mentioned in Section 3.3. The resulting phase angle responses are shown in Figure 5. The phase angle responses are linear with frequency over the range considered (0 to 2 c.p.s.) and this corresponds to simple time shifts in the data. In the case of the incidence vane and normal accelerometer systems this represents a data time shift (reference 17) of 1/40 second. The phase angle relationship for the pitch rate gyroscope corresponds to a data time shift of 1/31 second. The elevator deflection was measured by a linear potentiometer and should therefore have negligible errors due to instrument dynamics.

The corrections related to the dynamics of the instrumentation system were incorporated as time shifts of the data. As the data was sampled at discrete time intervals of 1/50 seconds, it was convenient to approximate the corrections by moving the incidence and normal acceleration channels forward by 1/50 second (instead of 1/40 second) and moving the pitch rate channel forward by 1/25 second (instead of 1/31 second).

In addition, the aerodynamic response of the windvane to a pulse input was measured in flight in smooth air at the test height and airspeed. The resulting damped oscillation of the windvane is shown in figure 7.

The windvane was found to have the following aerodynamic characteristics:

Relative damping	0.048
Undamped natural frequency (c.p.s.)	23.40

The frequency range of interest for frequency response testing of aircraft is usually less than 3 c.p.s., which is well below the vane natural frequency, and hence the aerodynamics of the vane result in no appreciable phase lag in the system.

Aerodynamic position error of incidence vane

The error resulting from the distortion of the airflow direction by the aircraft at the vane position consists of two parts, namely the static position error and the unsteady position error.

The windvane was found, from steady glide tests, to measure 1.25 times the actual incidence of the aircraft as shown in Figure 8. The unsteady position error is basically due to lag in the growth of lift. Immediately after a sudden increase in incidence the full incremental lift is not generated as the disturbed airflow takes a finite time to re-establish itself. The full upwash will therefore not be established and the windvane will under-read with respect to the uncorrected static values. This effect is zero at zero frequency (where the total position error equals the static position error), and increases with frequency so as to reduce the total position error. In Reference 13, Ridland gives some idea of the magnitude of the unsteady position error for a Meteor 7 aircraft for which the static position error is only reduced by one-tenth at a frequency of 5 c.p.s. Hence for the region of the short period frequency of the 'Dove' aircraft (approximately 0.5 c.p.s.), this unsteady effect can be neglected.

Errors due to geometrical positions of instruments

Kinematic errors arise from a pitch rate contribution due to the incidence and normal accelerations being measured at positions away from the aircraft centre of gravity.

Incidence

For a windvane situated a distance ℓ_v forward of the aircraft centre of gravity, the error in the incidence due to the aircraft pitch rate is:

$$\Delta\alpha = \frac{q\ell_v}{V}$$

Thus the correct expression for incidence at the aircraft centre of gravity is:

$$\alpha_{C.G.} = k_\alpha \alpha_v - \frac{q\ell_v}{V}$$

where k_α = static position error = 0.8

$$V = \frac{150 \text{ knots}}{\sqrt{\sigma}_{7000'}} \times 1.69 = 281 \text{ ft/sec. (T.A.S.)}$$

and, ℓ_v (FLTS. 7 and 8) = 15.87 feet

ℓ_v (FLTS. 9 and 10) = 15.03 feet.

Hence for flights 7 and 8, $\alpha_{C.G.} = 0.8\,\alpha_v - 0.056q$

and for flights 9 and 10, $\alpha_{C.G.} = 0.8\,\alpha_v - 0.053q$

where α is in degrees and q is in deg./sec.

Normal acceleration

For an accelerometer situated a distance ℓ_n forward of the aircraft centre of gravity, the error in the normal acceleration due to pitch rate of the aircraft is:

$$\Delta n = \frac{\dot{q}\ell_n}{g} + \frac{q^2 z_n}{g}$$

the latter term for small C.G. heights, Z_n, being neglected. Thus the correct expression for normal acceleration at the aircraft centre of gravity is:

$$n_{C.G.} = n_i - \frac{\dot{q}\ell_n}{g}$$

wherein Δq = difference between values of q at a sampling frequency of 50 times per second.

Hence for flights 7 and 8: $n_{C.G.} = n_i + \Delta q/738$

and for flights 9 and 10: $n_{C.G.} = n_i + \Delta q/41.30$

The corrections resulting from the dynamic calibrations and the position errors of the instrumentation were applied to the data tapes, using a simple programme on the Ferranti 'Pegasus' computer.

Appendix III

Frequency-response function for an arbitrary input

The transient response x(t) to a step function input applied at time, t = 0 may be approximated by a series of steps, as shown in figure 12. These steps occur at times

$$\frac{\Delta t}{2}, \frac{3\Delta t}{2}, \frac{5\Delta t}{2}, \ldots,$$

and have magnitudes, $\Delta x = x_1$, $\Delta x_2 = x_2 - x_1$, $\Delta x_3 \quad x_3 - x_2$, ..., where $x_1, x_2, x_3, \ldots$, are the magnitudes of the response at times Δt, $2\Delta t$, $3\Delta t$, ... As is shown in Reference 15 the frequency-response function may then be expressed in series form as:

$$f(i\omega) = Re^{i\alpha} = \Delta x_1 e^{-i\omega \frac{\Delta t}{2}} + \Delta x_3 e^{i\omega \frac{3\Delta t}{2}} \qquad (1)$$

With the frequency expressed in deg./sec. for convenience, the real and imaginary parts of the frequency-response function are:

$$\left.\begin{aligned} R_e = R\cos\alpha &= \sum_{r=1}^{q-1} \Delta x_r \cos\left(\frac{180}{\pi} r\omega \frac{\Delta t}{2}\right), \ r \text{ odd} \\ Im = R\sin\alpha &= -\sum_{r=1}^{q-1} \Delta x_r \sin\left(\frac{180}{\pi} r\omega \frac{\Delta t}{2}\right), \ r \text{ odd} \end{aligned}\right\} \qquad (2)$$

The frequency-response function for an arbitrary input may be found by writing:

$$F(i\omega) = \frac{\text{Output}}{\text{Arbitrary input}}(i\omega)$$

$$= \frac{\text{Output}}{\text{Step Input}}(i\omega) \Big/ \frac{\text{Arbitrary Input}}{\text{Step Input}}(i\omega) \qquad (3)$$

or, expressed in real and imaginary parts:

$$F(i\omega) = \frac{h(\omega) + i\,k(\omega)}{\ell(\omega) + i\,m(\omega)} \qquad (4)$$

wherein,

$$h(\omega) = \sum_{r=1}^{q-1} \Delta x_r \cos\left(r\frac{.180}{\pi} .\omega.\frac{\Delta t}{2}\right)$$

$$k(\omega) = -\sum_{r=1}^{q-1} \Delta x_r \sin\left(r\frac{.180}{\pi}.\omega.\frac{\Delta t}{2}\right)$$

$$\ell(\omega) = \sum_{r=1}^{q-1} \Delta\theta_r \cos\left(r\frac{.180}{\pi}.\omega.\frac{\Delta t}{2}\right) \qquad (5)$$

$$m(\omega) = -\sum_{r=1}^{q-1} \Delta\theta_r \sin\left(r\frac{.180}{\pi}.\omega.\frac{\Delta t}{2}\right)$$

where r is odd.

Rationalising equation (4) and expressing it in real and imaginary parts yield:

$$F(i\omega) = a(\omega) + ib(\omega) \qquad (6)$$

where,

$$a(\omega) = \frac{h\ell + km}{\ell^2 + m^2}$$

$$b(\omega) = \frac{k - hm}{\ell^2 + m^2} \qquad (7)$$

Then the required amplitude ratio and phase difference of output to input are:

$$R(\omega) = (a^2 + b^2)^{\frac{1}{2}}$$

$$\alpha(\omega) = \tan^{-1}\left(\frac{b}{a}\right) \qquad (8)$$

Thus equations (8) represent the frequency-response of a system to an arbitrary input.

Appendix 4

Harmonic content of triangular inputs

The frequency range over which accurate transformations can be obtained is determined by the shape of the control input. Theoretically, a pure impulse (zero time duration) is the most desirable input for all purposes because it gives uniform excitation to the entire frequency spectrum. The transform of a step input has a magnitude that varies inversely with frequency and therefore gives infinite excitation to the zero frequency component at the expense of the higher frequencies.

In practice it is necessary for the input to put some energy into the system (the aircraft) and therefore the input must have a finite time duration. The nearest approach to a pure impulse therefore is an input that is triangular in shape as shown in figure 42.

Now if 'a' is the slope and T the time base of the triangular input then the Fourier transformation of the input is given by:

$$\delta(i\omega) = \int_0^T \delta(t)\, e^{-i\omega t} dt$$

Integration results in a transformation with the following real and imaginary parts:

$$R = \frac{2a}{\omega^2} \cos\frac{\omega T}{2}\left(1 - \cos\frac{\omega T}{2}\right)$$

$$I = \frac{2a}{\omega^2} \sin\frac{\omega T}{2}\left(\cos\frac{\omega T}{2} - 1\right)$$

The magnitude of the transformation is then

$$|\delta| = \frac{2a}{\omega^2}\left(1 - \cos\frac{\omega T}{2}\right)$$

For the case of this report in which the Fourier transformation is based on the derivative of the input as follows:

$$\delta(i\omega) = \int_0^T \delta'(t) e^{-i\omega t} dt$$

then integration results in a transformation with the following real and imaginary parts:

$$R' = -\frac{2a}{\omega}\sin\frac{\omega T}{2}\left(\cos\frac{\omega T}{2} - 1\right)$$

$$I' = \frac{2a}{\omega}\cos\frac{\omega T}{2}\left(1 - \cos\frac{\omega T}{2}\right)$$

The magnitude of the transformation being:

$$|\delta'| = \frac{2a}{\omega}\left(1 - \cos\frac{\omega T}{2}\right)$$

It may be seen that the magnitude of the transformation for both the case where the input time history is used and the case where the derivative of the input time history is used is periodic and equal to zero when $\omega = n4\pi/T$, $(n = 1,2, \ldots,)$.

The magnitudes of the transformation for both cases are shown in figure 42 for triangular inputs of 0.5 and 1.0 second duration respectively. The amplitudes of the triangular inputs are chosen to be inversely proportional to their duration so that the areas under the triangles are equal. This ensures, in the case of the transformation using the input time history itself, that the magnitudes of the transforms are equal at zero frequency.

Appendix 5

Theoretical frequency responses

In considering the short period frequency range of the aircraft, the generalized equations of motion can be simplified by neglecting both the elevator lift and the phugoid freedom.

As shown by Ridland in reference 16, responses computed on this simple basis are reasonably correct in the case of tailed aircraft for frequencies near the short period frequency whereas with tail-less aircraft it is advisable to include the effects of elevator lift.

The simplified equations of motion with respect to stability axes together with the assumptions governing them are as follows:-

Assumptions

1. Speed is constant (no phugoid mode).
2. The aircraft is trimmed in level flight.
3. There is no coupling with lateral modes.
4. The aircraft is rigid.
5. Elevator lift is neglected, and
6. The system is linear.

Equations of motion

$$(D - Z_w)\left(\frac{w}{V}\right) - q\hat{t} = 0$$

$$-\left\{\frac{m_w^{\bullet}}{i_B}D + \frac{\mu m_w}{i_B}\right\}\left\{\frac{w}{V}\right\} + \left\{D - \frac{m_q}{i_B}\right\}q\hat{t} - \frac{\mu m\eta_\eta}{i_B} = 0 \qquad (1)$$

Frequency response formulae incidence, $\left(\frac{w}{V}\right)$

The aircraft incidence frequency response is given by:

Modulus

$$\left|\frac{\left(\frac{w}{V}\right)}{-\eta}\right| = \left|\frac{\delta}{C}\,\frac{1}{[(1-x^2) + (2\zeta x)^2]^{\frac{1}{2}}}\right| \qquad (2)$$

Phase lag (of incidence behind negative elevator)

$$\phi_{\left(\frac{w}{V}\right)} = \tan^{-1}\left(\frac{2\zeta x}{1-x^2}\right) \qquad (3)$$

It is apparent from equations (2) and (3) that the incidence frequency response is of exactly the same form as that of a simple, one degree of

freedom, mass-spring-damper system. Examples of these frequency response curves, which are uniquely defined by the non-dimensional frequency, x, and the damping ratio, ζ, are shown in Figure 42. Use has been made of the fact that the phase lag is always 90 degrees at the natural damped frequency, x = 1, in order to match the measured and theoretical responses. The value C can be estimated from the measured response and the value of B determined from the damping ratio, ζ. With B and C known, δ, the elevator moment coefficient, can then be evaluated.

Normal acceleration, n

The aircraft frequency response in terms of normal acceleration at the centre of gravity is given by:

Modulus

$$\left|\frac{n}{-\eta}\right| = \frac{a\rho SV^2}{2W} \frac{\delta}{C} \left|\frac{1}{[(1-x^2)^2 + (2\zeta x)^2]^{\frac{1}{2}}}\right| \qquad (4)$$

Phase lag

$$\phi_n = \tan^{-1}\left(\frac{2\zeta x}{1-x^2}\right) \qquad (5)$$

Apart from the constant, $\frac{a\rho SV^2}{2W}$, in the expression for the modulus these are identical to those for incidence response.

Rate of pitch q

The rate of pitch frequency response is given by:

Modulus

$$\left|\frac{q}{-\eta}\right| = \left|\frac{a\rho SV}{2W} g \frac{\delta}{C} \left[\frac{1 + \left(\frac{x}{2\zeta_a}\right)^2}{(1-x^2)^2 + (2\zeta x)^2}\right]^{\frac{1}{2}}\right| \qquad (6)$$

Phase lag

$$\phi_q = \tan^{-1}\left[\frac{(4\zeta\zeta_a + x^2 - 1)x}{2\zeta_a(1-x^2) + (2\zeta x^2)}\right] \qquad (7)$$

The frequency response curves in this case are also defined by the non-dimensional frequency, x, the damping ratio ζ, and an additional parameter ζ_a which is the damping ratio due to the heaving motion alone.

Thus from frequency response measurements it is possible to evaluate B, C, a and δ and hence $(m_q + m_{\dot{w}})$, m_w in terms of m_q, and m_η.

The inclusion of the elevator lift term, $- Z_{\eta}\eta$, in the equations of motion is such that the system no longer corresponds to a simple spring-mass-damper system. The effects of elevator lift on the frequency responses are also described by Ridland in reference 16. However, for a highly damped aircraft such as the test aircraft of this report, the effects of elevator lift in the region of the short period frequency are small and well within the experimental errors involved.

References

1. Greenberg, H. — 'A survey of methods for determining stability parameters of an airplane from dynamic flight measurements'. NACA T.N. 2340, April 1951.

2. Eggleston, J.M. Mathews, C.W. — 'Application of several methods for determining transfer functions and frequency response of aircraft from flight data'. NACA Report 1204, 1954.

3. Crane, H.L. — 'A manual frequency sweep technique for the measurement of airplane frequency response'. NASA T.N. D-375, April 1960.

4. Shinbrot, M. — 'A least squares curve fitting method with applications to the calculation of stability coefficients from transient-response data. NACA T.N. 2341, April 1951.

5. Donegan, J.J. Pearson, H.A. — 'Matrix method of determining the longitudinal stability coefficients and frequency response of an aircraft from transient flight data. NACA Report 1070, 1952.

6. Triplett, W.C. Brown, S.B. Smith, G.A. — 'The dynamic-response characteristics of a 35° swept-wing airplane as determined from flight measurements'. NACA Report 1250, 1955.

7. LaVerne, M.E. Boksenbom, A.S. — 'Frequency response of linear systems from transient data'. NACA Report 977, 1950.

8. Cole, H.A., Jr. Crown, S.C. Holleman, E.C. — 'Experimental and predicted longitudinal and lateral-directional response characteristics of a large flexible 35° swept-wing airplane at an altitude of 35,000 feet'. NACA Report 1330, August 1957.

9. Shinbrot, M. — 'On the analysis of linear and non-linear dynamical systems from transient-response data'. NACA T.N. 3288, December 1954.

10. Press, H. Tukey, J.W. — 'Power spectral methods of analysis and their application to problems in airplane dynamics'. AGARD Flight Test Manual, Volume 4.

11. Houbolt, J.B.
Steiner, R.
Pratt, K.G.
'Dynamic response of airplanes to atmospheric turbulence including flight data on input and response'.
NASA TRR-199, June 1964.

12. McLaren, J.
'Calibration methods for the accurate assessment of some flight test instruments.
ARC CP 760, 1964.

13. Ridland, D.M.
'Unsteady lift slope values obtained from flight measurements in gusts'.
ARC CP 651, 1963.

14. Bennett, G.E.
'The role of magnetic recording in aircraft instrumentation'.
RAE T.R. 64077, December, 1964.

15. Rushton, E.
Medhurst, M.G.
'Routine computing method for approximating to the frequency response from the transient response'.
RAE T.N. I.A.P. 1083, July, 1959.

16. Ridland, D.M.
'The longitudinal frequency response to elevator of an aircraft over the short period frequency range'.
ARC CP. 476, 1960.

17. Wolowicz, C.H.
Holleman, E.C.
'Stability derivative determination from flight data'.
AGARD Report 224, October 1958.

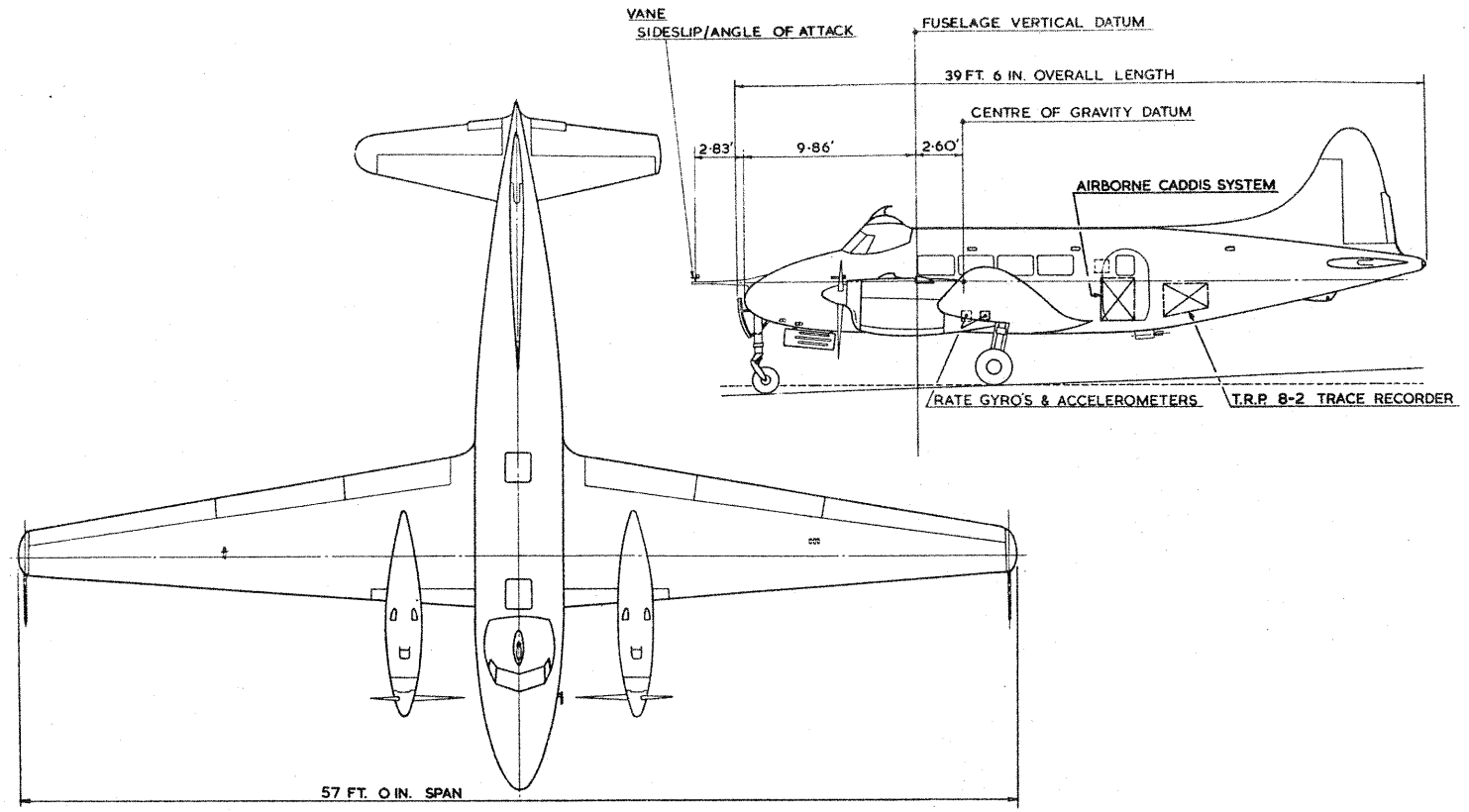

FIGURE. 1.

DOVE 5 AIRCRAFT – G-AMXW

GENERAL ARRANGEMENT AND LOCATION OF INSTRUMENTATION SYSTEMS.

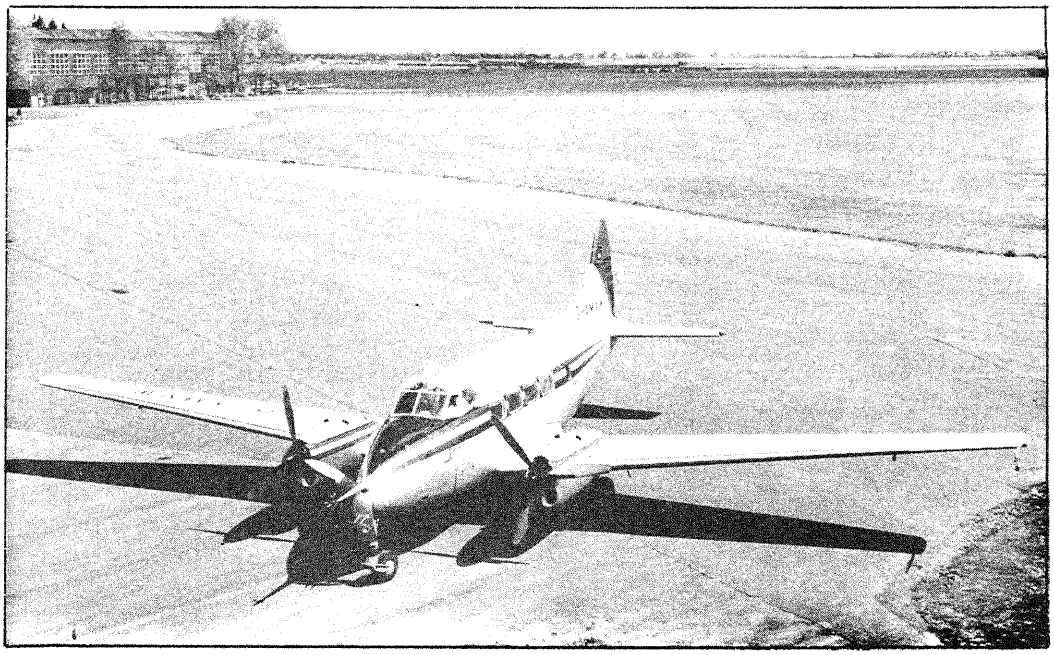

FIG. 2. THE HAWKER SIDDELEY 'DOVE' 5
TEST AIRCRAFT.

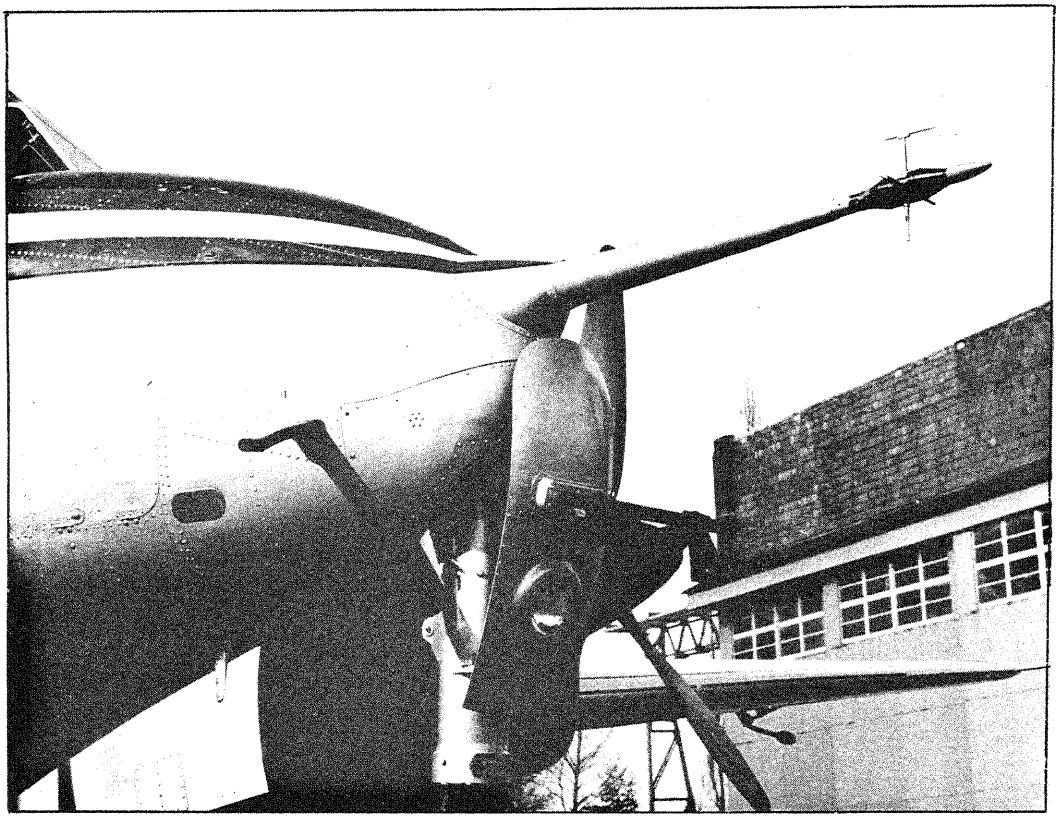

FIG. 3. INSTALLATION OF ANGLE-OF-ATTACK

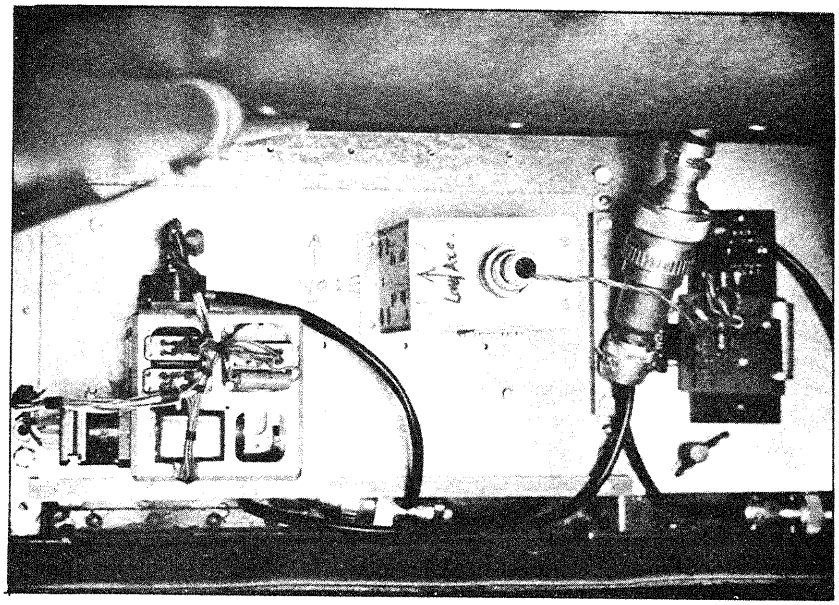

FIG. 4. NORMAL ACCELEROMETER AND PITCH RATE GYROSCOPE INSTALLATION.

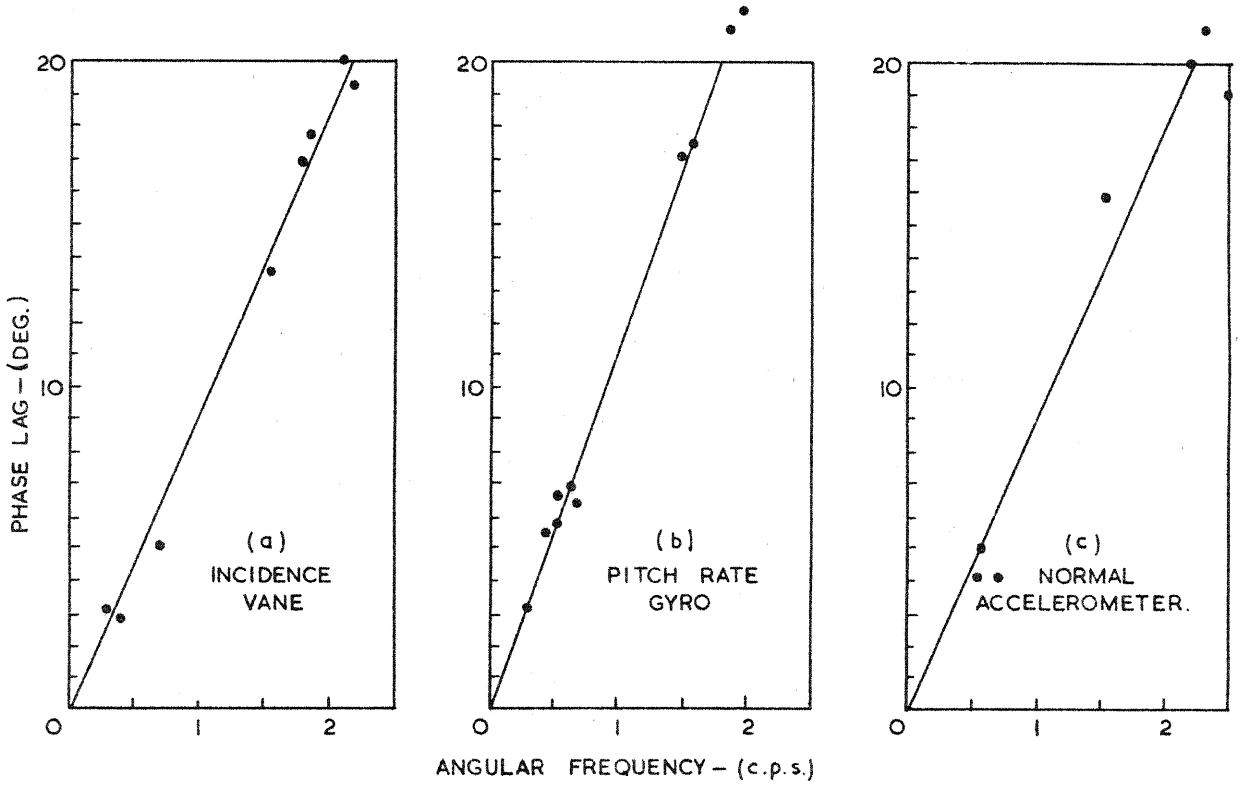

FIG. 5. INSTRUMENTATION PHASE ANGLE RESPONSES.

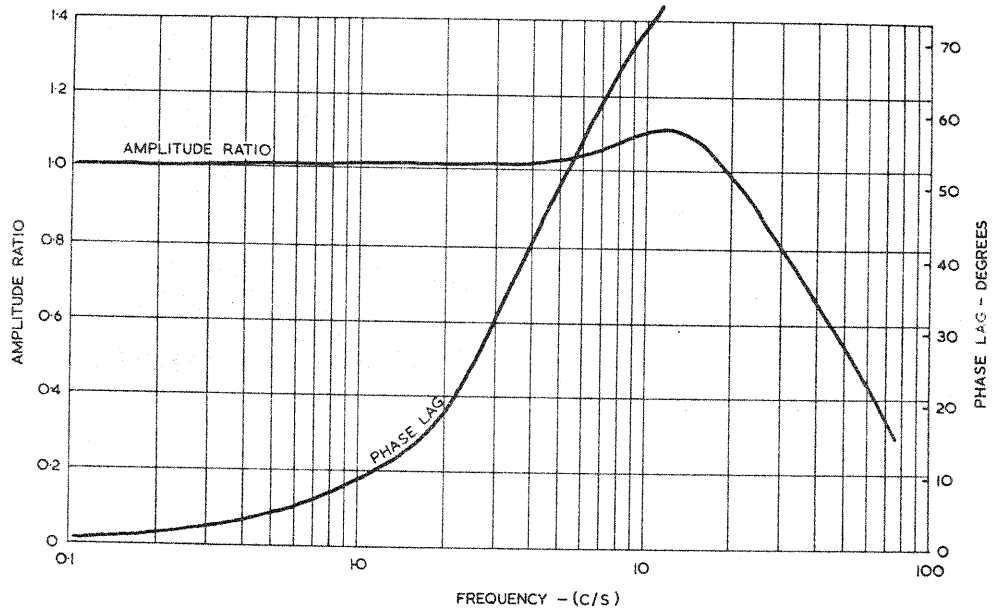

FIG. 6. NORMAL ACCELEROMETER DYNAMIC RESPONSE

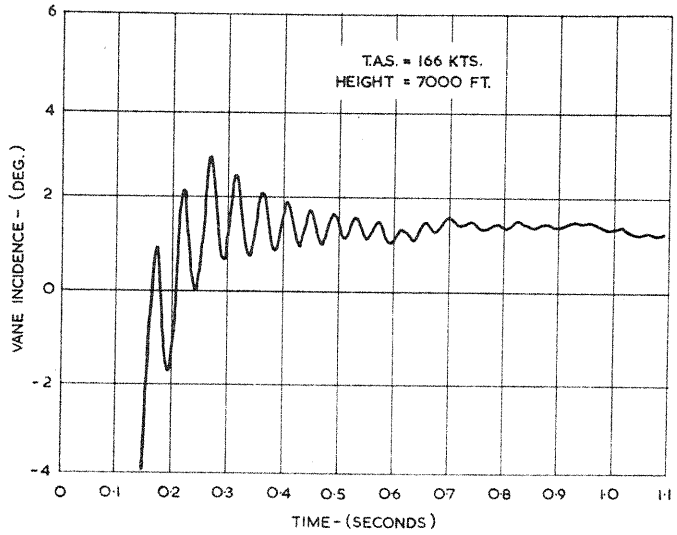

FIG. 7. WINDVANE TRANSIENT RESPONSE TO A PULSE INPUT.

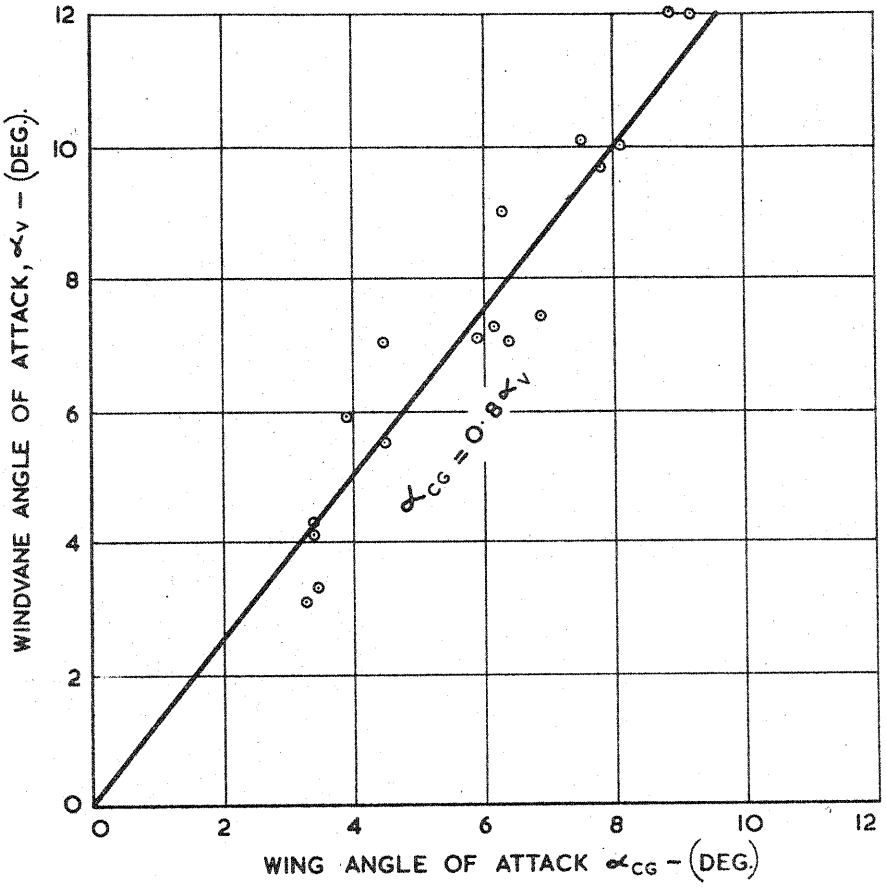

FIG.8. WINDVANE STATIC CALIBRATION 'DOVE' G-AMXW.

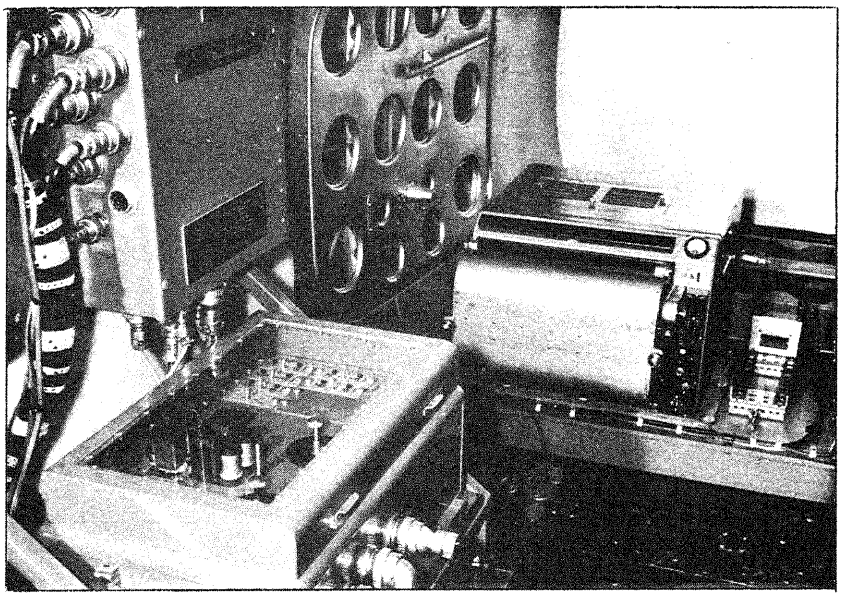

FIG. 9. INSTALLATION OF MAGNETIC TAPE RECORDER AND GALVANOMETER TRACE RECORDER IN TEST AIRCRAFT.

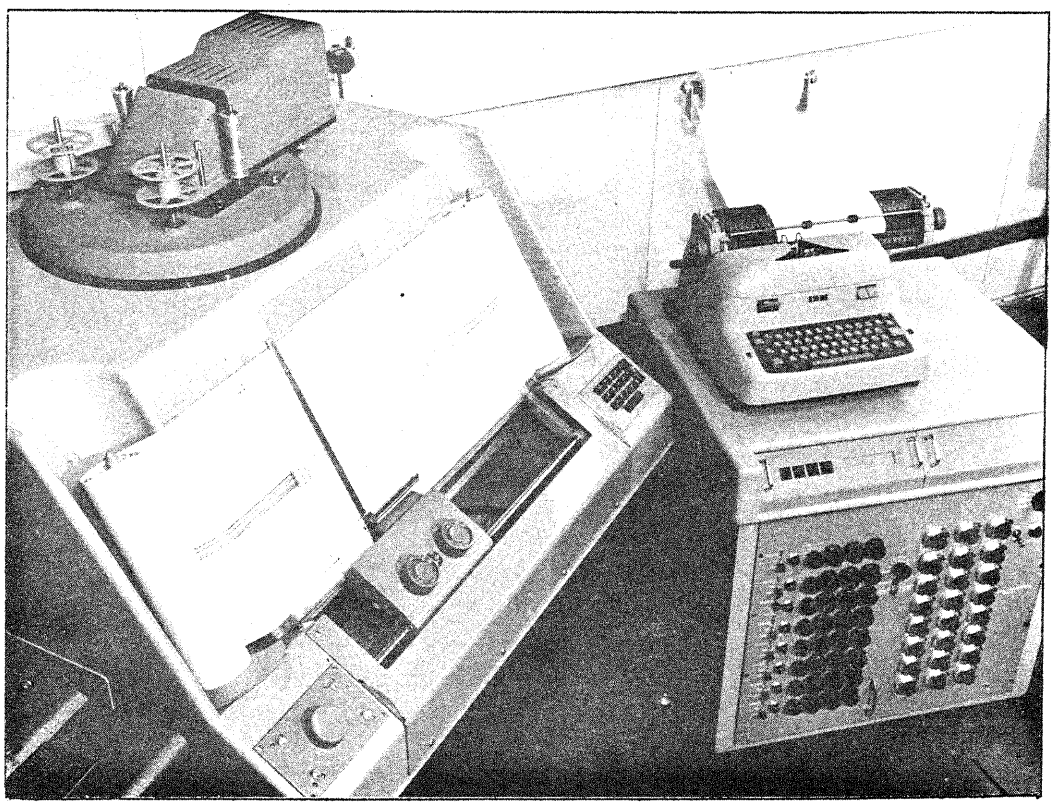

FIG. 10. BENSON LEHNER 'OSCAR' TRACE READER.

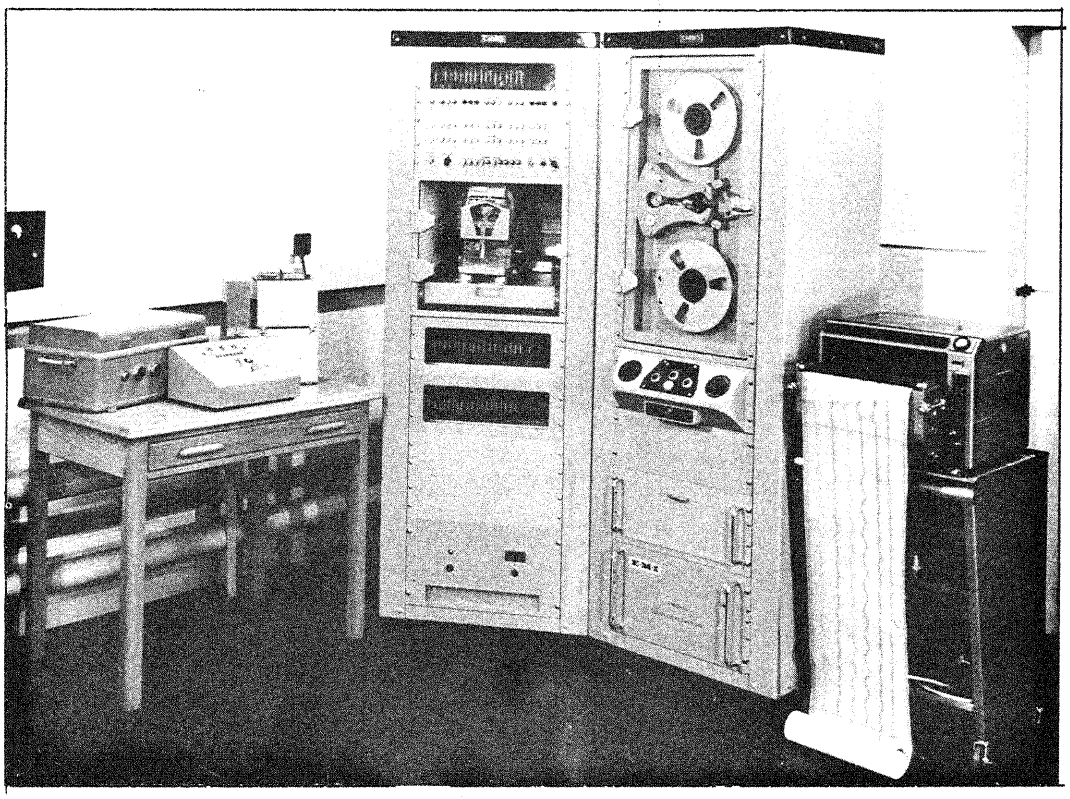

FIG. 11. CADDIS — THE GROUND SYSTEM.

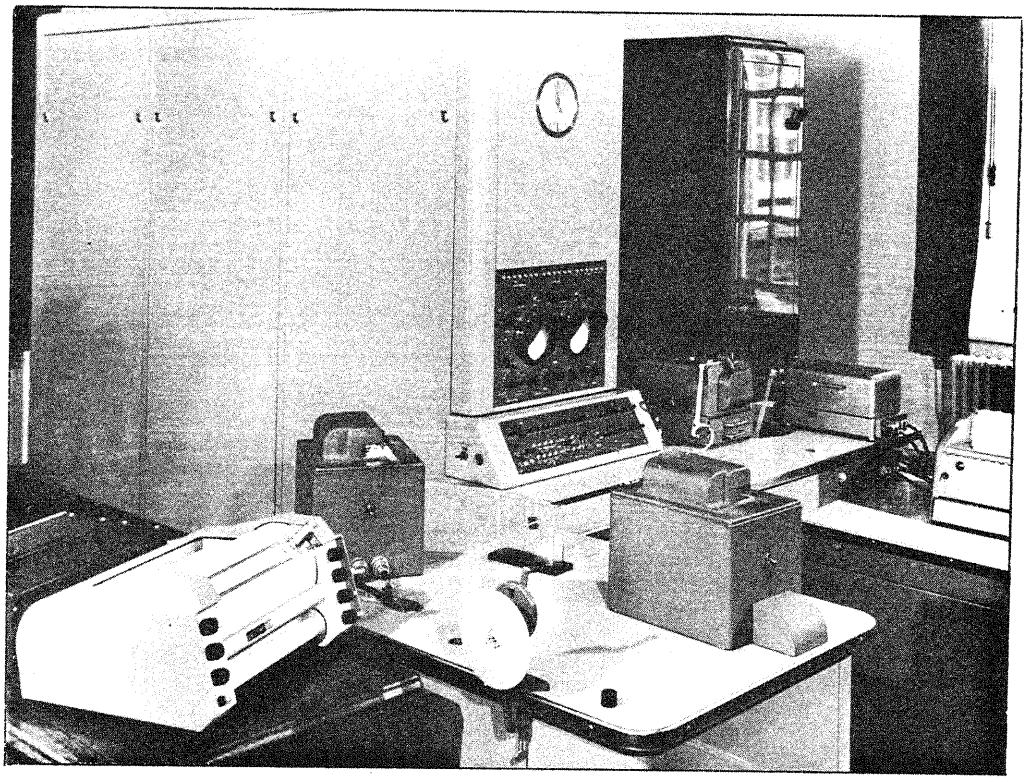

FIG. 12. FERRANTI PEGASUS DIGITAL COMPUTER

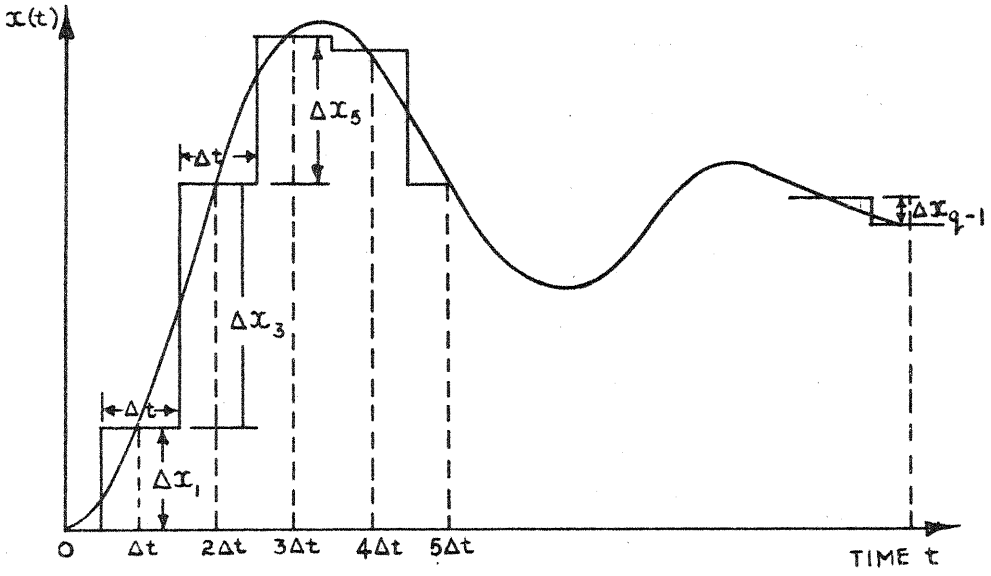

FIG. 13. APPROXIMATION OF A TRANSIENT RESPONSE, $x(t)$, BY A SERIES OF INCREMENTAL STEPS.

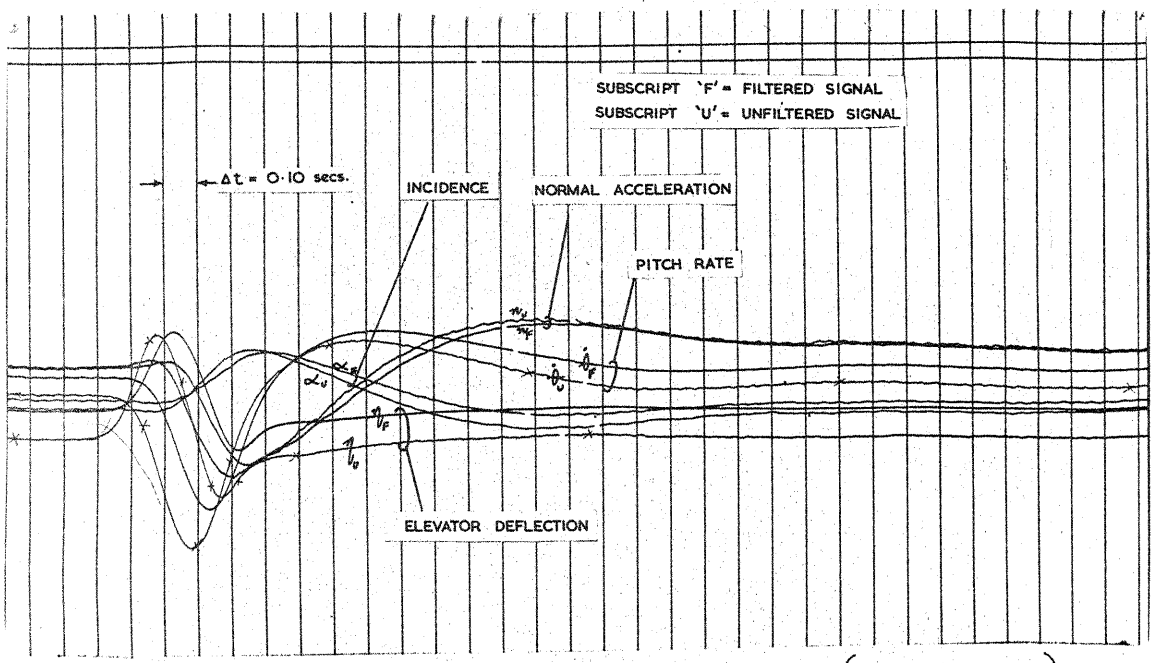

FIG.14. A TYPICAL GALVANOMETER TRACE RECORD (FLT. 7, RUN 5.)

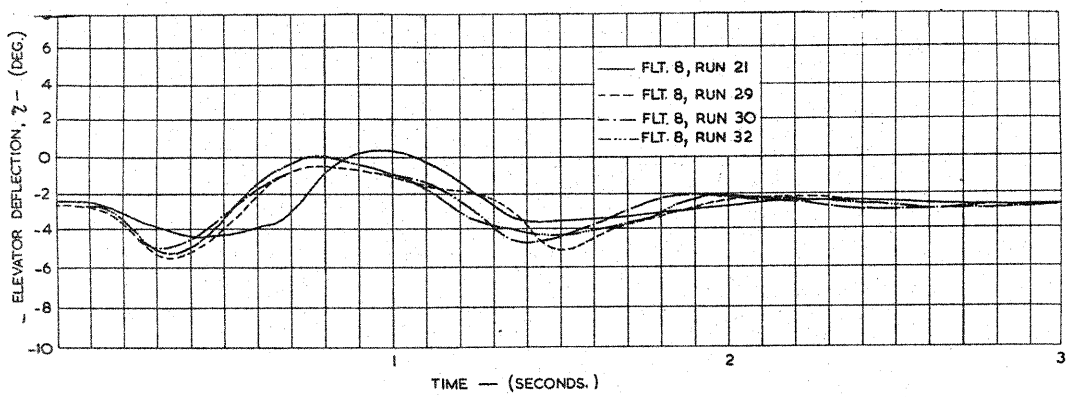

FIG. 15. ELEVATOR INPUT TIME HISTORIES.

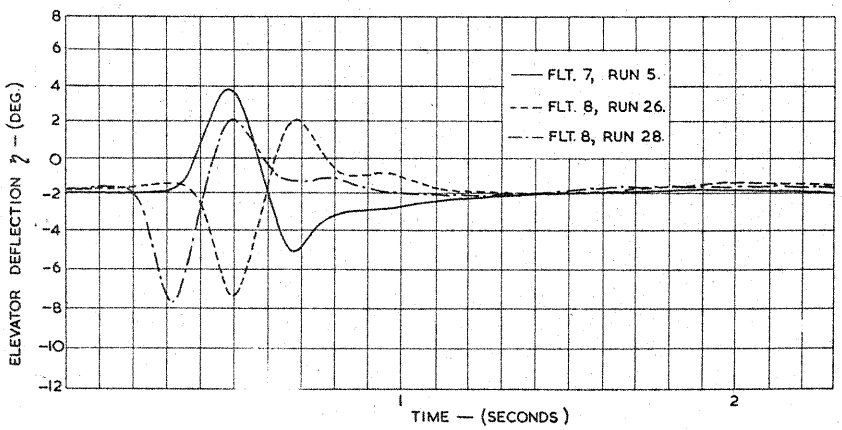

FIG. 16. ELEVATOR INPUT TIME HISTORIES.

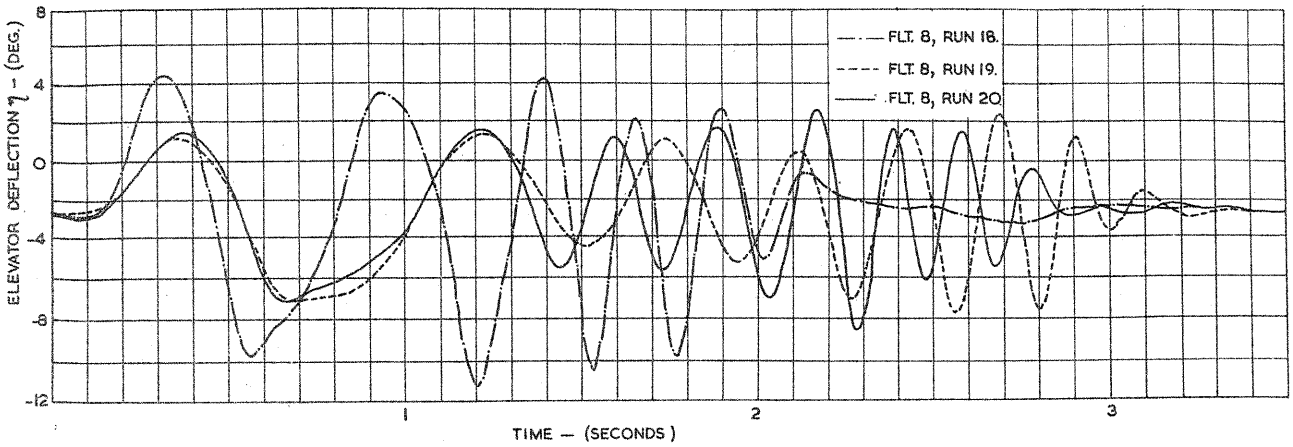

FIG. 17. ELEVATOR INPUT TIME HISTORIES.

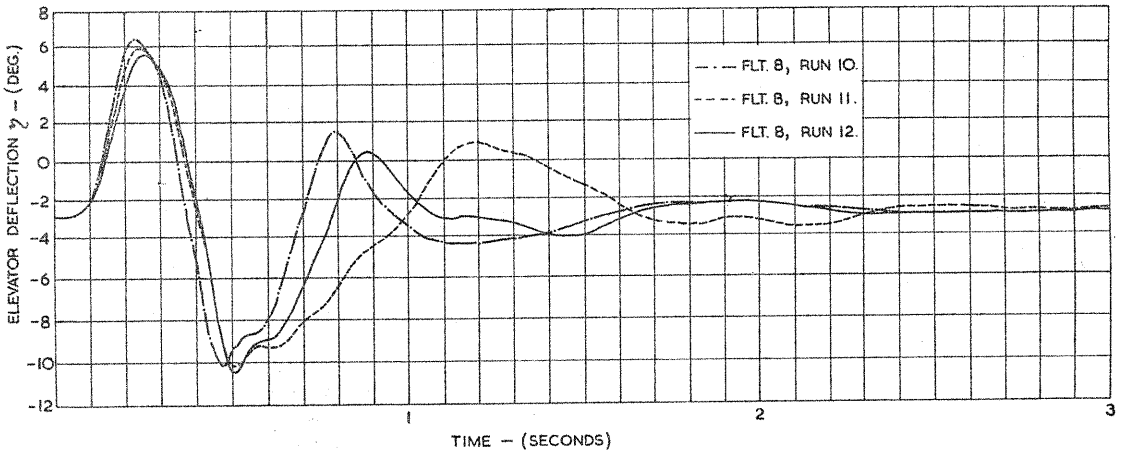

FIG. 18. ELEVATOR INPUT TIME HISTORIES.

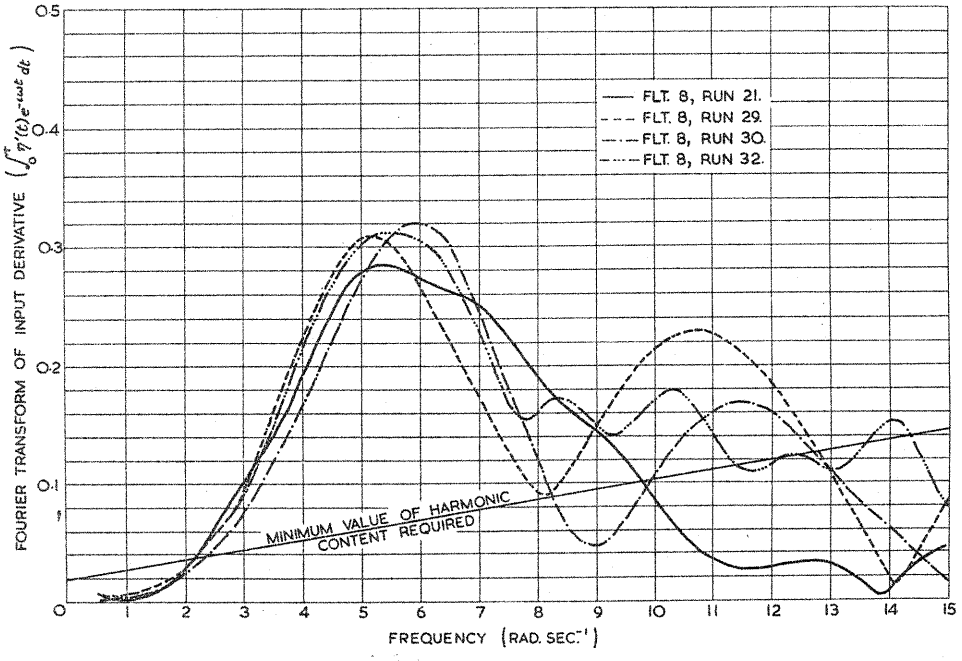

FIG.19. HARMONIC CONTENTS OF THE ELEVATOR INPUTS OF FIGURE. 15

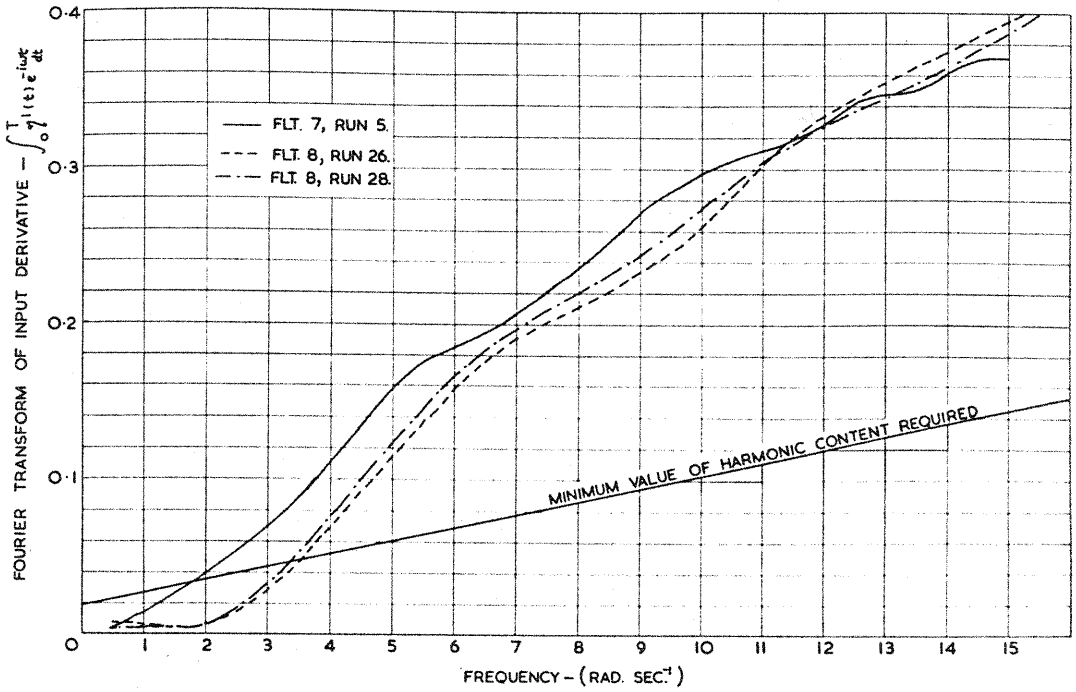

FIG.20. HARMONIC CONTENTS OF THE ELEVATOR INPUTS OF FIGURE. 16.

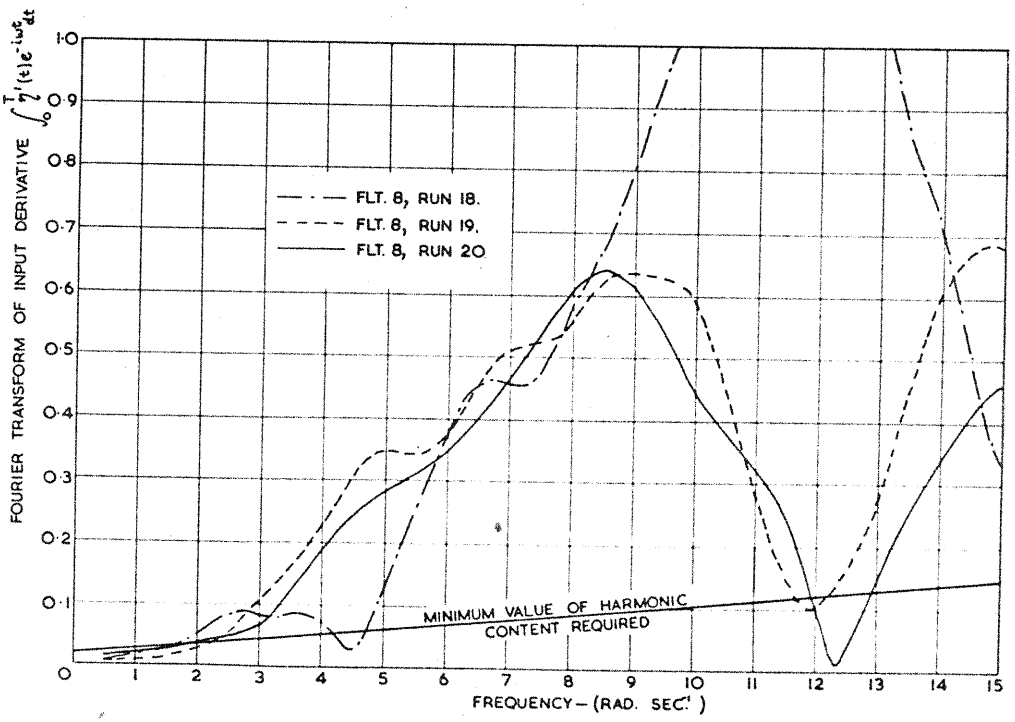

FIG.21. HARMONIC CONTENTS OF THE ELEVATOR INPUTS OF FIGURE. 17.

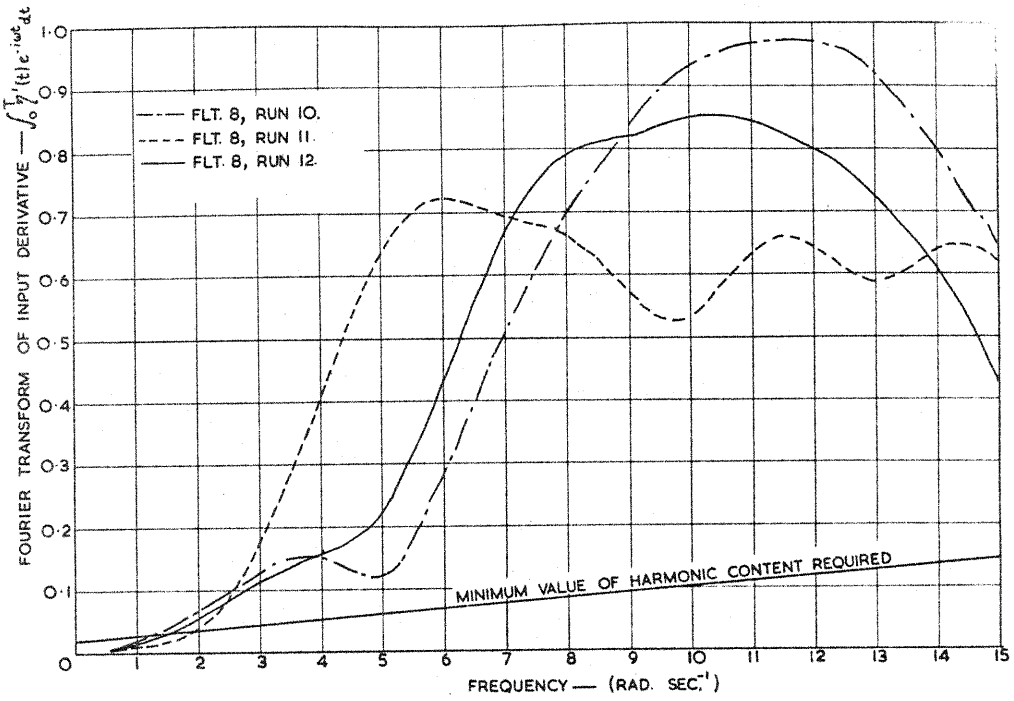

FIG.22. HARMONIC CONTENTS OF THE ELEVATOR INPUTS OF FIGURE. 18.

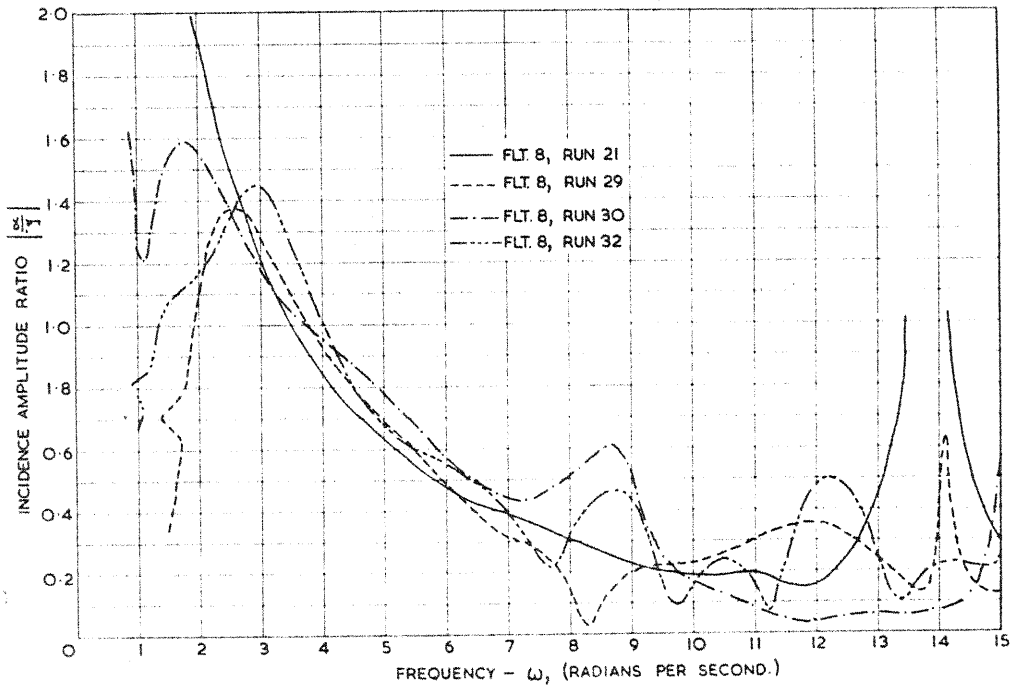

FIG.23. INCIDENCE AMPLITUDE RATIO FREQUENCY RESPONSES.

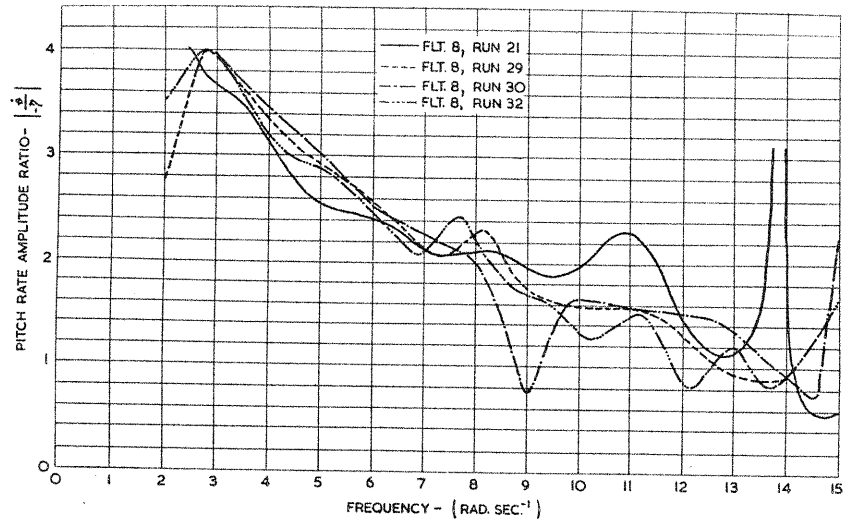

FIG.24. PITCH RATE AMPLITUDE RATIO FREQUENCY RESPONSES.

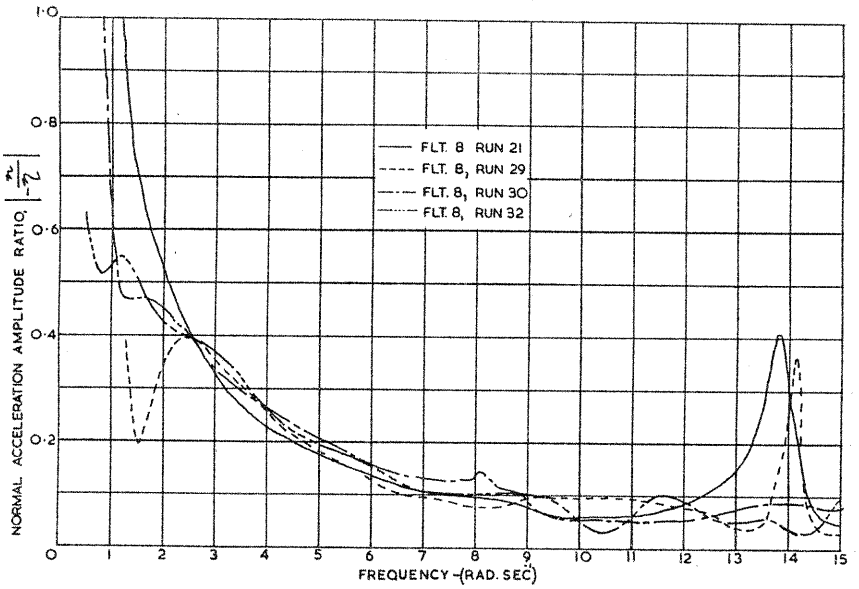

FIG.25. NORMAL ACCELERATION AMPLITUDE RATIO FREQUENCY RESPONSES.

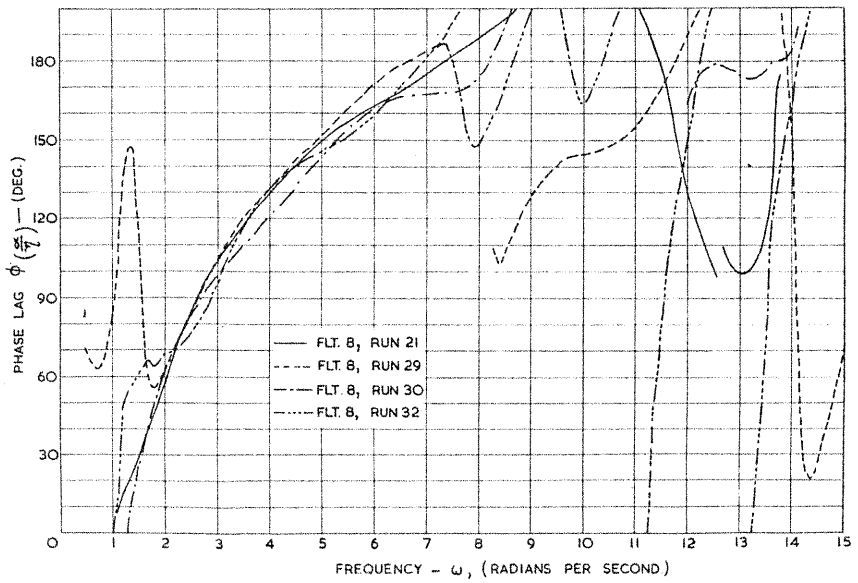

FIG.26. INCIDENCE PHASE ANGLE FREQUENCY RESPONSE.

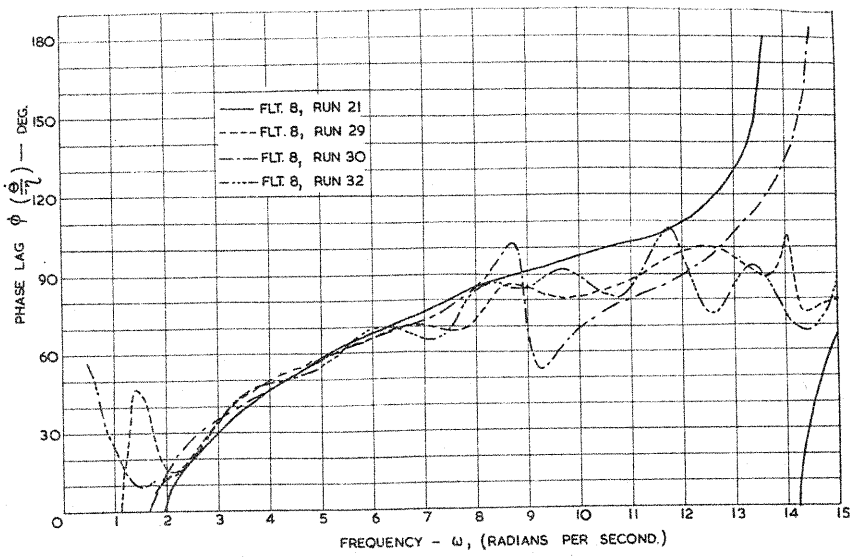

FIG.27. PITCH RATE PHASE ANGLE FREQUENCY RESPONSE.

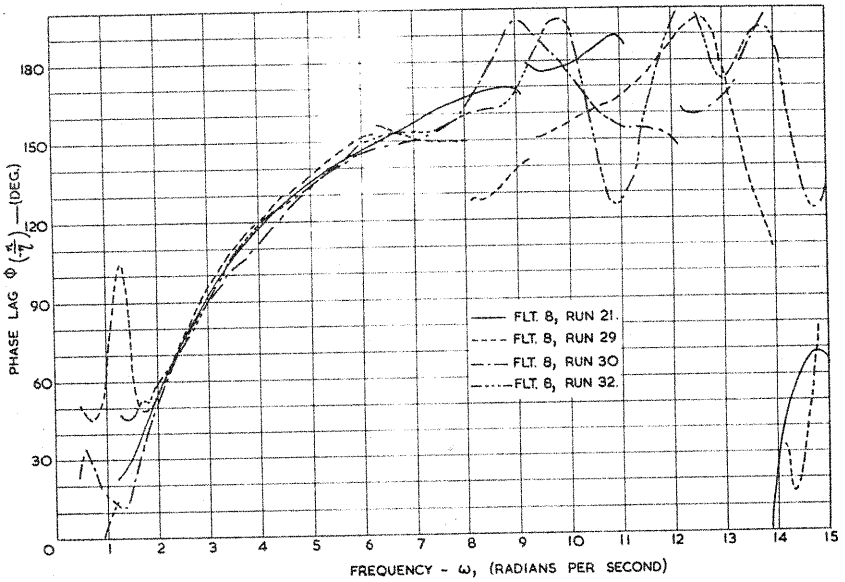

FIG.28. NORMAL ACCELERATION PHASE ANGLE FREQUENCY RESPONSE.

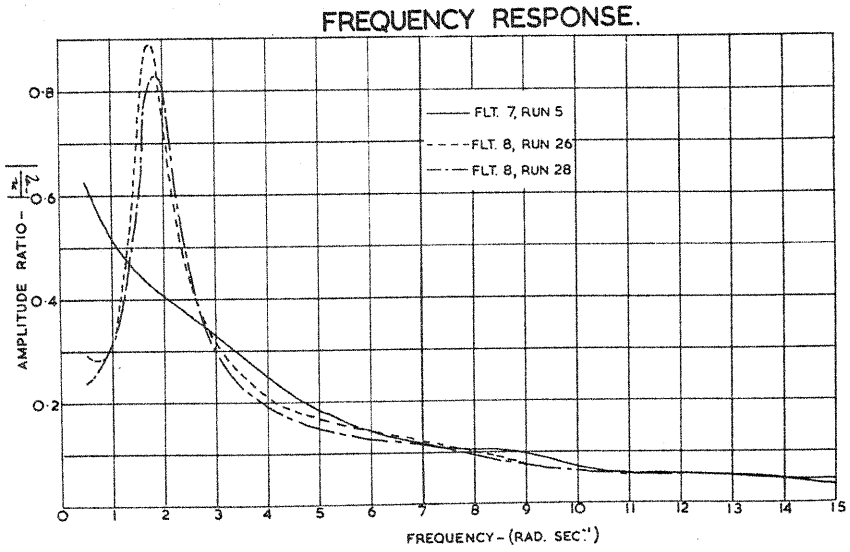

FIG.29. NORMAL ACCELERATION AMPLITUDE RATIO FREQUENCY RESPONSE.

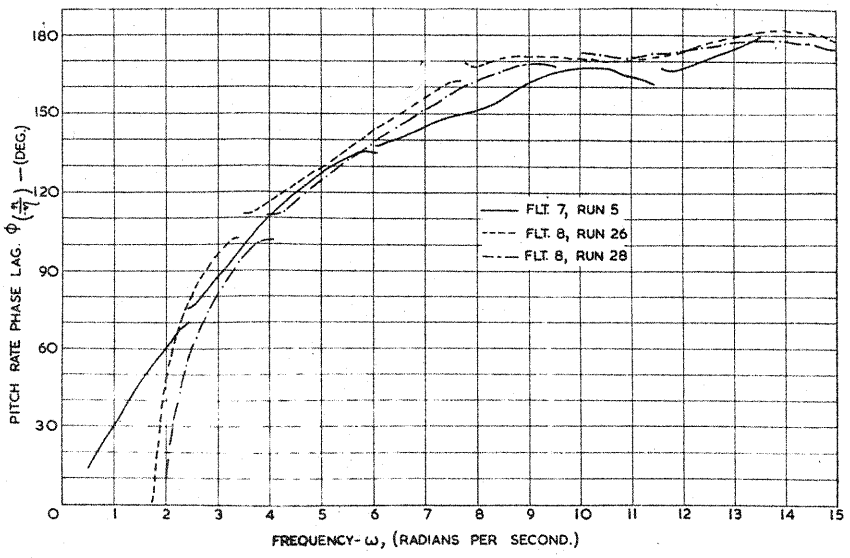

FIG.30. NORMAL ACCELERATION PHASE ANGLE FREQUENCY RESPONSE.

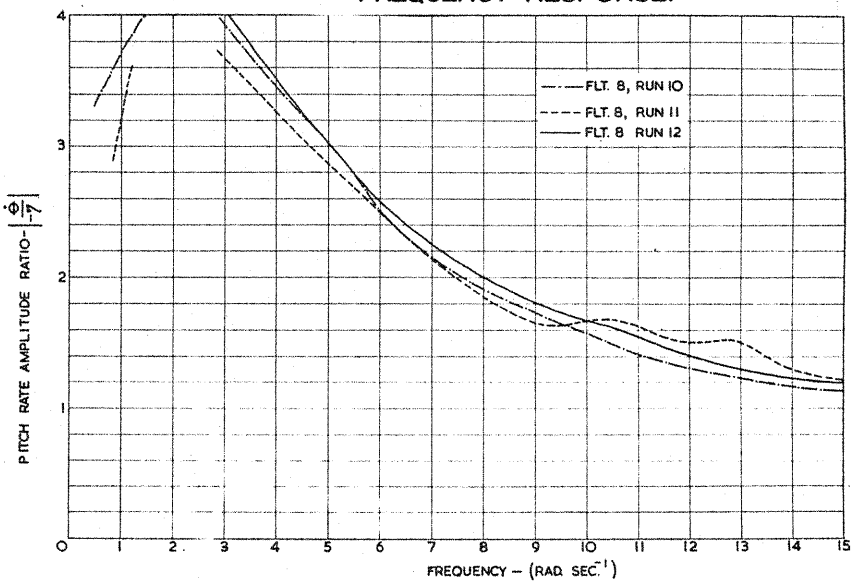

FIG.31. PITCH RATE AMPLITUDE RATIO FREQUENCY RESPONSE.

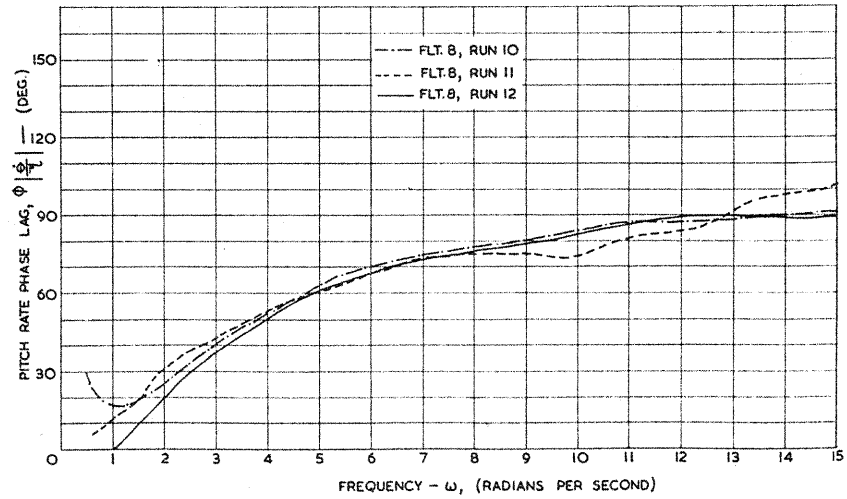

FIG.32. PITCH RATE PHASE ANGLE FREQUENCY RESPONSE.

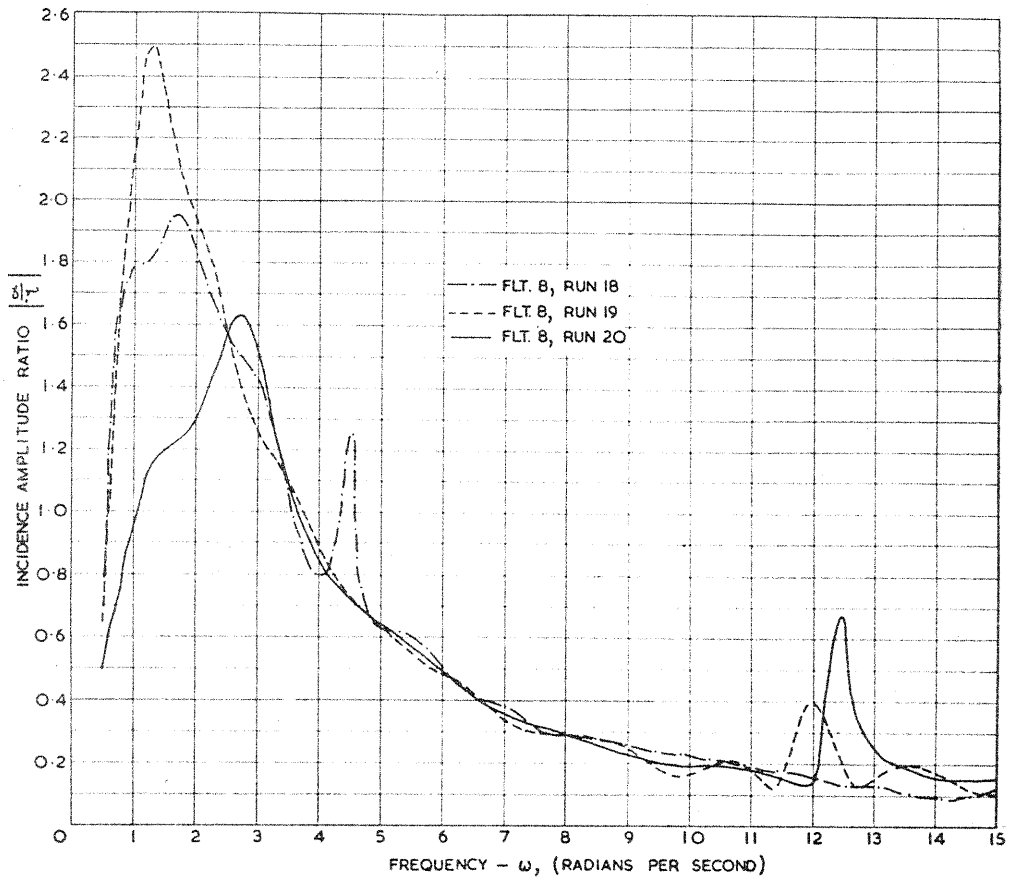

FIG.33. INCIDENCE AMPLITUDE RATIO FREQUENCY RESPONSE.

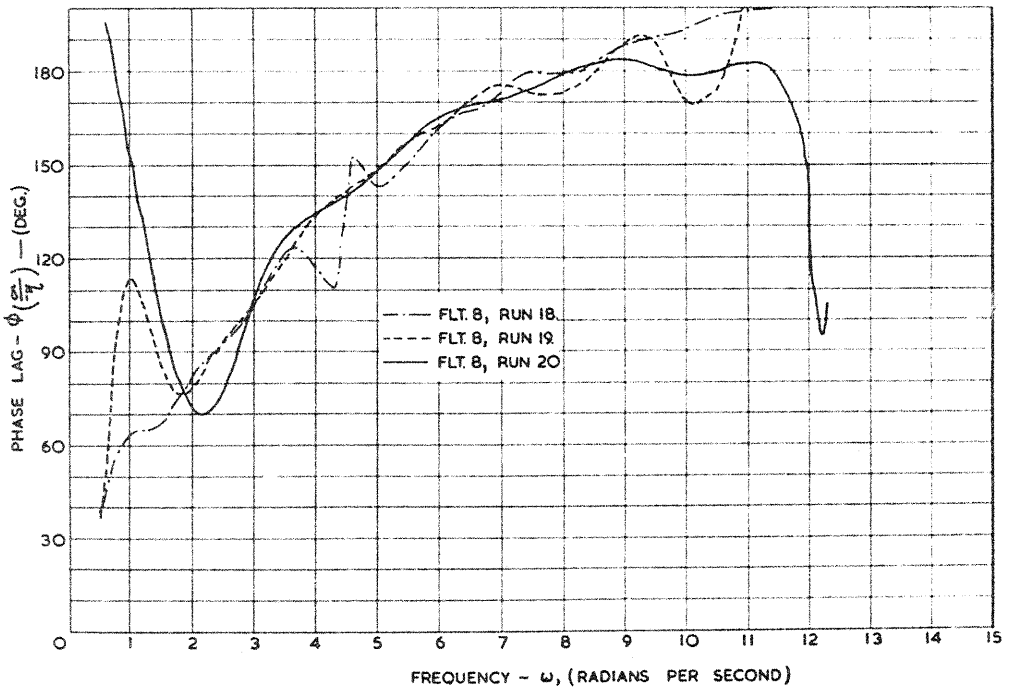

FIG.34. INCIDENCE PHASE ANGLE FREQUENCY RESPONSE.

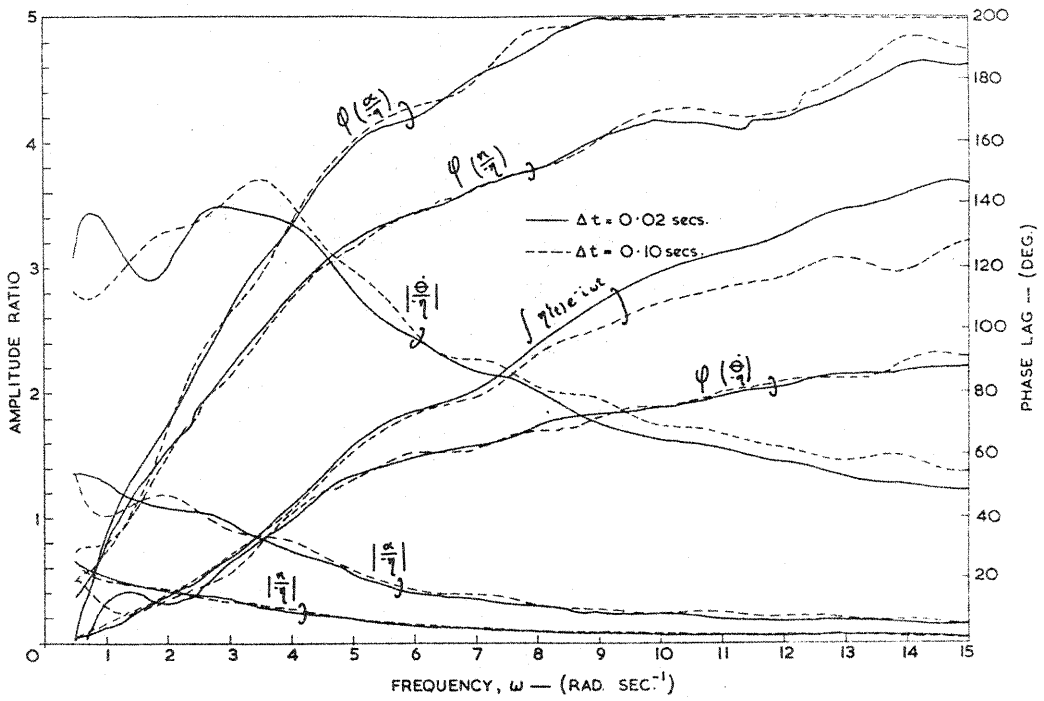

FIG. 35. EFFECT OF DATA SAMPLING TIME INTERVAL ON FREQUENCY RESPONSE (FLT. 7, RUN 5.)

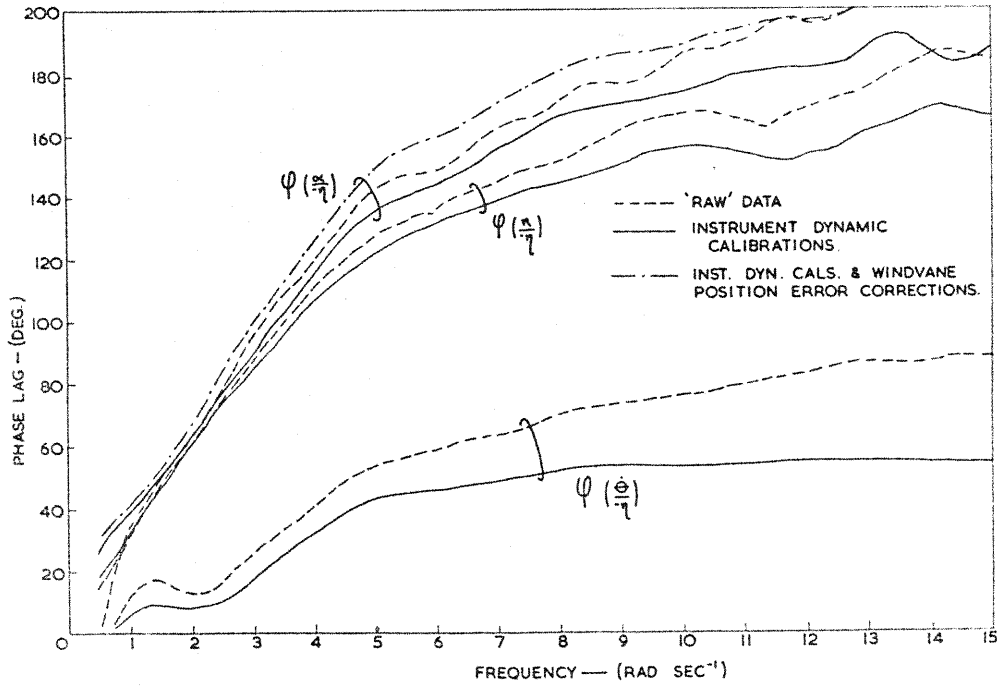

FIG. 36. THE EFFECT OF INSTRUMENTATION CALIBRATIONS ON THE PHASE ANGLE RESPONSE (FLT. 7, RUN 5)

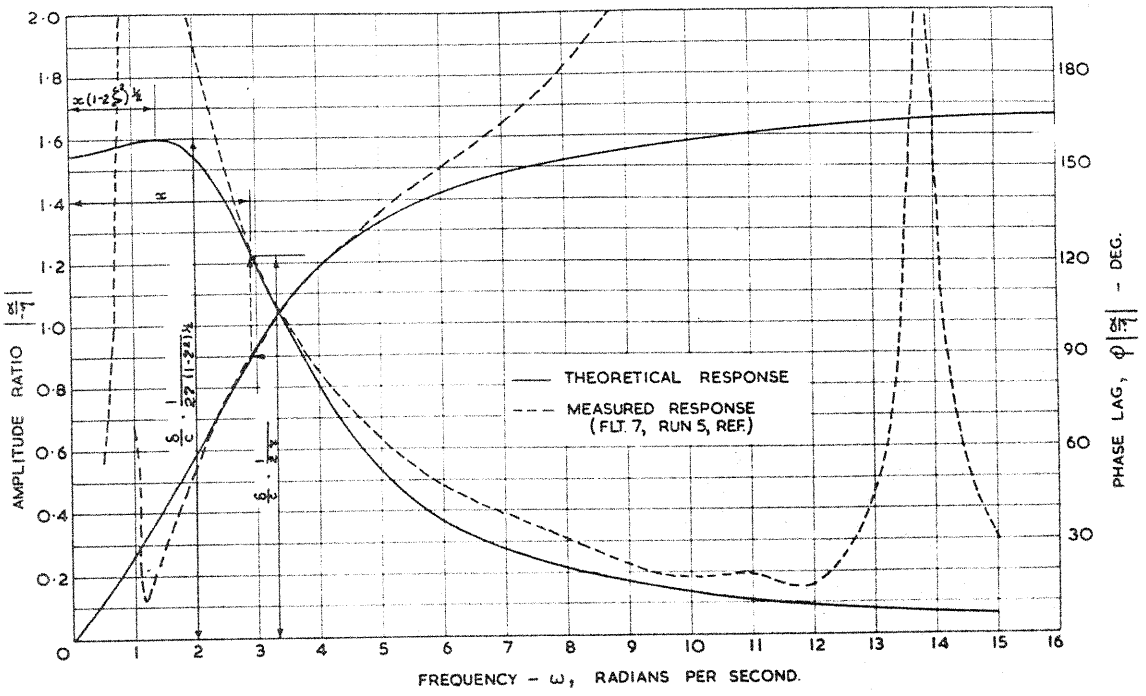

FIG.37. A COMPARISON OF MEASURED AND THEORETICAL. INCIDENCE FREQUENCY RESPONSES.

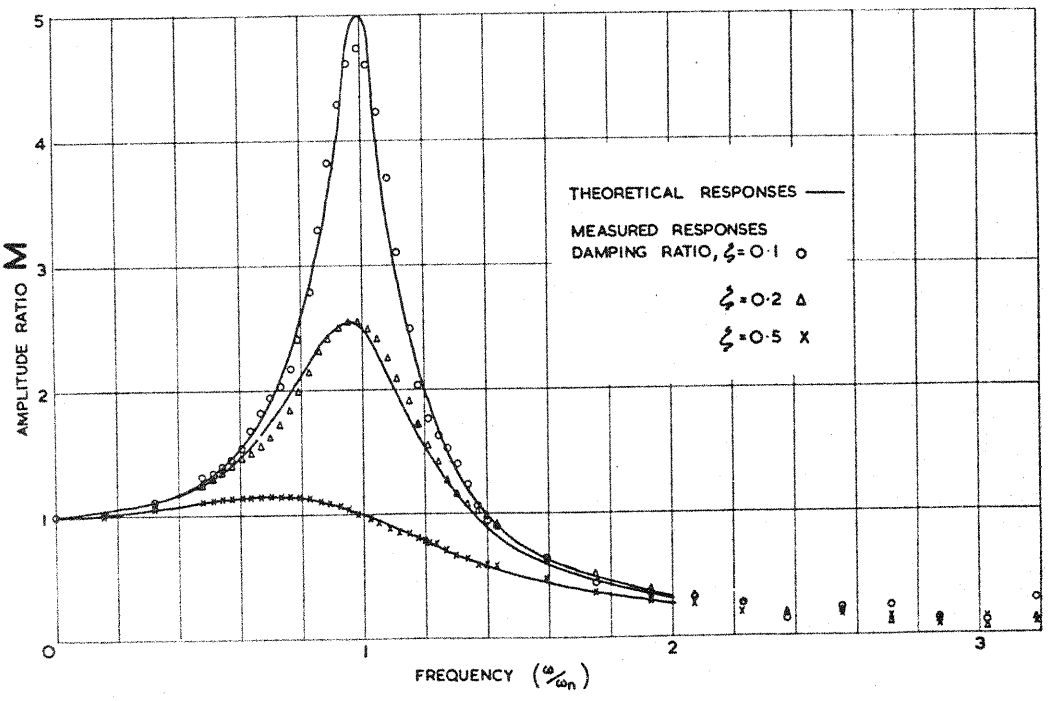

FIG.38. MEASURED AND CALCULATED AMPLITUDE RATIO FREQUENCY RESPONSES OF A SECOND ORDER SYSTEM.

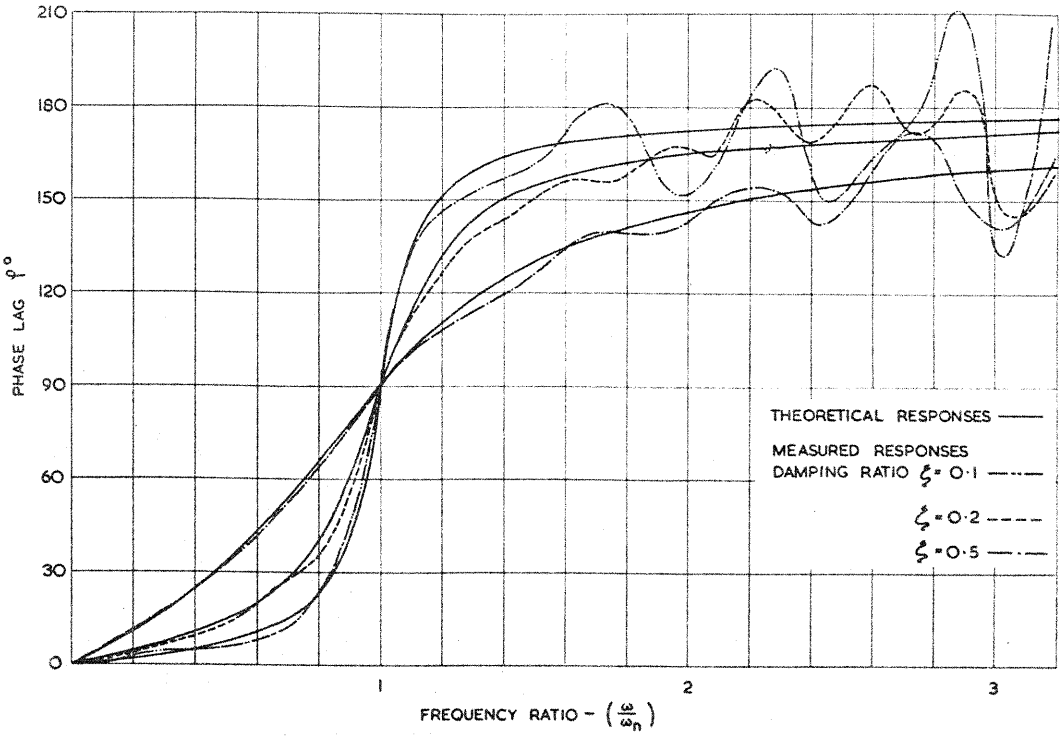

FIG.39. MEASURED AND CALCULATED PHASE ANGLE FREQUENCY RESPONSES OF A SECOND ORDER SYSTEM.

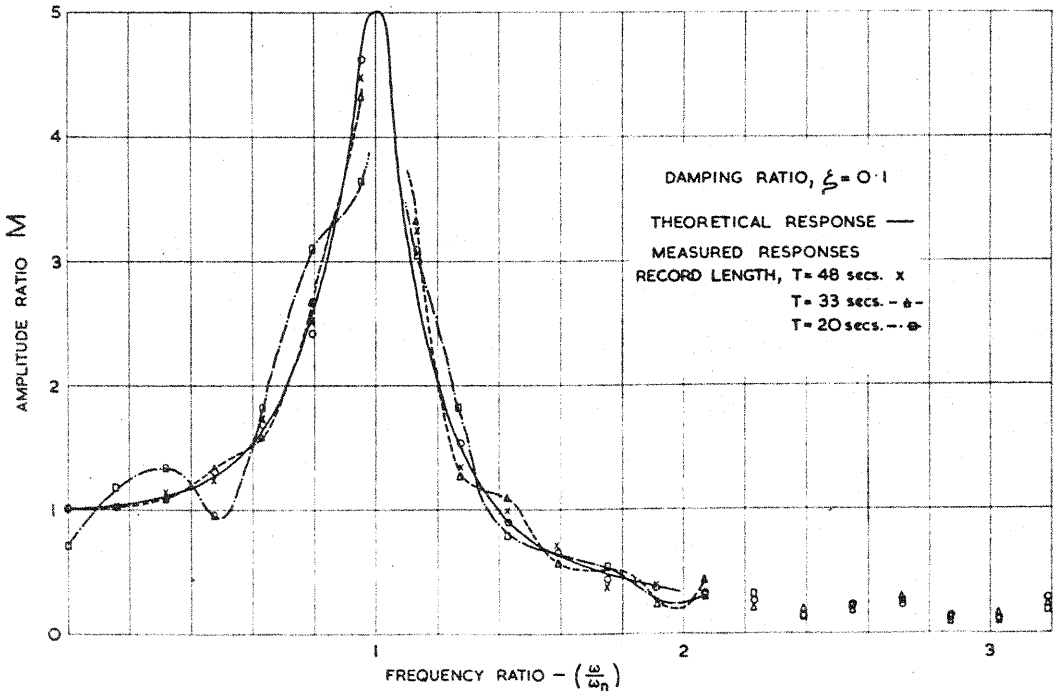

FIG.40. EFFECT OF TRUNCATION OF RECORD LENGTH ON THE MEASURED AMPLITUDE RATIO FREQUENCY RESPONSES OF A SECOND ORDER SYSTEM.

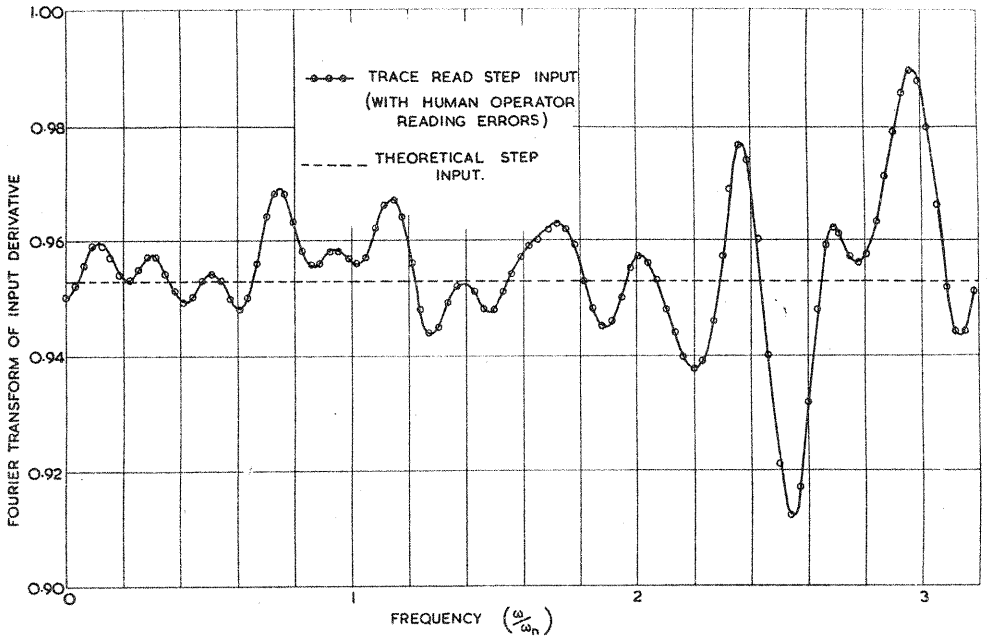

FIG.41. FOURIER TRANSFORM OF THE DERIVATIVE OF TRACE READ STEP INPUT.

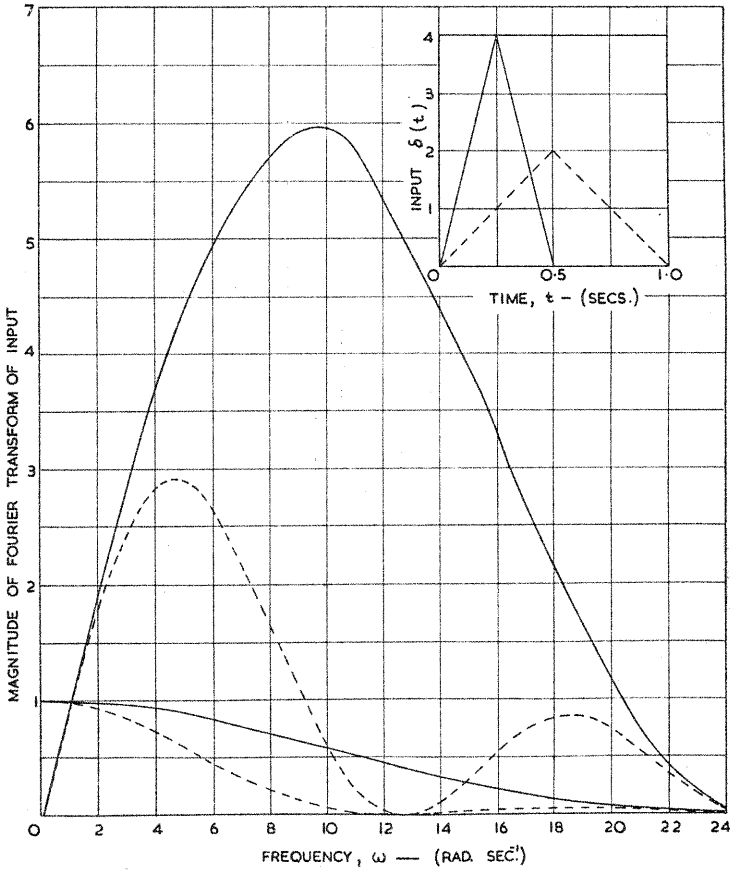

FIG.42. FOURIER TRANSFORM MAGNITUDES OF TWO TRIANGULAR INPUTS FOR THE FORMS OF THE TRANSFORMATION, $(i\omega) = \int_0^T \delta\ (t) e^{-i\omega t}.dt.$ AND $\delta(i\omega) = \int_0^T \delta^1\ (t) e^{-i\omega t}.dt.$